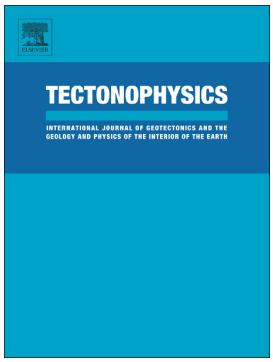

Systematic assessment of fault stability in the Northern Niger Delta Basin, Nigeria: Implication for hydrocarbon prospects and increased seismicities

E.O. Adewole, D. Healy

PII: S0040-1951(17)30051-3
DOI: doi: 10.1016/j.tecto.2017.02.005
Reference: TECTO 127397

To appear in: *Tectonophysics*

Received date: 4 October 2016
Revised date: 30 January 2017
Accepted date: 6 February 2017

Please cite this article as: E.O. Adewole, D. Healy , Systematic assessment of fault stability in the Northern Niger Delta Basin, Nigeria: Implication for hydrocarbon prospects and increased seismicities. The address for the corresponding author was captured as affiliation for all authors. Please check if appropriate. Tecto(2017), doi: 10.1016/j.tecto.2017.02.005

Systematic assessment of fault stability in the Northern Niger Delta Basin, Nigeria: Implication for hydrocarbon prospects and increased seismicities

E.O. Adewole, D. Healy

Department of Geology and Petroleum Geology, School of Geosciences, Meston Building, King's College, University of Aberdeen, Aberdeen, AB24 3UE, United Kingdom

ABSTRACT

Accurate information on fault networks, the full stress tensor, and pore fluid pressures are required for quantifying the stability of structure-bound hydrocarbon prospects, carbon dioxide sequestration, and drilling prolific and safe wells, particularly fluid injections wells. Such information also provides essential data for a proper understanding of superinduced seismicities associated with areas of intensive hydrocarbon exploration and solid minerals mining activities. Pressure and stress data constrained from wells and seismic data in the Northern Niger Delta Basin (NNDB), Nigeria, have been analysed in the framework of fault stability indices by varying the maximum horizontal stress direction from 0^o to 90^o, evaluated at depths of 2 km, 3.5 km and 4 km. We have used fault dips and azimuths interpreted from high resolution 3D seismic data to calculate the predisposition of faults to failures in three faulting regimes (normal, pseudo-strike-slip and pseudo-thrust). The weighty decrease in the fault stability at 3.5 km depth from 1.2 MPa to 0.55 MPa demonstrates a reduction of the fault strength by high magnitude overpressures. Pore fluid pressures greater than 50 MPa have tendencies to increase the risk of faults to failure in the study area. Statistical analysis of stability indices (SI) indicates faults dipping 50^o - 60^o, 80^o - 90^o, and azimuths ranging 100^o - 110^o are most favourably oriented for failure to take place, and thus likely to favour migrations of fluids given appropriate pressure and stress conditions in the dominant normal faulting regime of the NNDB. A few of the locally assessed stability of faults show varying results across faulting regimes. However, the near similarities of some model-based results in the faulting regimes explain the stability of subsurface

structures are greatly influenced by the maximum horizontal stress (SH_{max}) direction and magnitude of pore fluid pressures.

Keywords: Niger Delta; fault failure; slip tendency; dilation tendency; fracture stability; earth tremors

1. Introduction

It will be a great mistake to understate the seriousness of a complete understanding of the fault strength as one of the key determinants of the structural stability in well casing designs, engineering constructions, hydrocarbon and mineral explorations, and predetermining the occurrence of destructive and extensive seismicity of high magnitude scales. We carried out this study in the onshore NNDB, Nigeria (Figure 1). A map view of wells located in the area is shown in Figure 2(A). An enlarged view of the portion studied in detail (area AZ1) is presented in Figure 2(B). Although virtually all the wells have good depth penetrations in most of the locations, but a greater number of them were missing complete log data (density, resistivity and sonic). By implication, detailed study was carried out in 13 wells that have good quality well data, and covered by high resolution (48-fold stack) 3D seismic data. The dominant normal faults interpreted from the seismic data have been modelled using appropriate pore fluid pressures (P_p) and stresses (ratio) constrained from the study area, and also from worldwide basins to simulate pseudo-strike-slip and pseudo-thrust faulting regimes. These approaches have allowed an in-depth assessment of the stability of faults in the three faulting regimes.

Oceanic and continental tectonics are capable of causing temporal changes in both the stress field and faulting regime. For instance, Ziegler (1992) linked a possible change in the stress field of Africa to the conceivable northward movement of the African continent, and ultimate collision with the Europe in the Late Cretaceous.

In this study, we determined the appropriate geomechanical conditions (pore fluid pressure, fault connection, and stress magnitude and direction) that are likely to cause faults to be unstable, and which contemporaneously may favour the migration of structure-bound fluid. This approach is hinged on the apparent determination of the optimum SH_{max} direction that may sustain stable structures in the subsurface. The estimated fault SI shows which part of the fault plane is more likely to slip (reactivate and break a seal), dilate (open and allow fluid to pass along the fault plane or cracks) or be unstable (failure). In this work, we have also used the SI to model faults in different faulting regimes by varying the direction of the SH_{max} by intervals of 15^o from 0^o to 90^o to compensate for any possible change in its orientation by tectonic and non-tectonic forces. Only the large faults; Figure 2(B), which were highly likely to be deep-set, and define the structural geometry of the study area were included in the models.

Anderson (1942) averaged dip values of growth faults in a typical sedimentary basin to 55^o. Nevertheless, in the Niger Delta Basin, the effect of gravitational forces has caused average fault dip angle to reduce considerably with depth up to 20^o or less (Weber, 1971). In this study, the interpreted faults show a dip range of 0^o to 90^o from the surface to the deep. The highest dip values were recorded in the shallow levels (less than 3 km), but as the faults flatten out, the dip of the faults tends towards zero. Greater than 12% of our modelled fault segments originated from shallow depths, and dipped between 70^o to 80^o (equivalent to 160^o - 190^o dip azimuth). It statistically enabled us to compare and emphasise differences between stability of faults in the shallow, intermediate and deep depths. All the models have distinct input data suitable for each depth, which led to more complete understanding of the structural stability investigated. The results of this study will have direct application to induced seismicity triggered by mining activities and production-driven wells.

2. Stratigraphy and tectonic history

Tectonically, the deformed part of the NNDB constitutes the landward extensional zone (normal faulting and simple rollover anticlines) and seaward compressional zone (strike-slip, thrust faulting and clay diapirs), which episodically formed during the Eocene to the present day (Weber and Daukoru, 1975). The entire Niger Delta Basin is prolific based on its significant proven hydrocarbon reserves, particularly within the deformed offshore part, where major hydrocarbon plays are anticlines and fault-bound footwall and hanging wall closures. The structural settings and depositional histories, the petrology of the three main lithological units (Benin, Agbada and Akata Formations), and hydrocarbon migration and trapping mechanisms have been comprehensively discussed by previous authors (Hospers, 1965, 1971; Stoneley, 1966; Short and Stauble, 1967; Weber, 1971, 1987; Burke, 1972; Merki, 1972; Weber and Daukoru, 1975; Avbovbo, 1978; Evamy et al., 1978; Whiteman, 1982; Doust and Omatsola, 1990; Adewole et al., 2016).

Sedimentations in the basin commenced southward from the Anambra Basin in the Late Cretaceous. Numerous regressive depositional cycles and a few transgressive from the Eocene to the present days sequenced unconsolidated sands (Benin Formation), intercalated sands and shales (paralic sequence; Agbada Formation) and prodeltaic marine shales (Akata formation) to the top, middle and bottom of the basin respectively. The Agbada Formation serves as the main reservoir rock for hydrocarbons. The very thick and undercompacted shales are responsible for the high magnitude overpressures observed in the basin (Figure 3; Adewole et al., 2016).

Because of the compounded effects of the rapid subsidence and limited compaction, there are concentrations of syndepositional growth faults with increasing steepness toward the Atlantic Ocean (Merki, 1972; Weber and Daukoru, 1975; Tuttle et al., 1999). These interpretations explain the source-diversity of sealing potentials of the faults basinwide, which have been reported influential to occurrences of commercial hydrocarbon accumulations (Evamy et al., 1978). Fault connections (soft and hard

links) observed from the seismic interpretation, as shown in Figure 2(B), have potentials to greatly influence trapping of fluids, and exert constraints on the fault slip, fracture orientation, sealing and fluid migration (Trudgill and Cartwright, 1994; Davies et al., 1997; Calvez et al., 2002). A hard link is generally impervious to fluid flow, whereas the soft link, contrastingly, permits, and also well-known to associate with commercial hydrocarbon reserves worldwide (Morley et al., 1990; Matthai et al., 1996). However, these links do not necessarily function as direct and automatic interpretations of the structural stability in depths because such approach is not only unreliable but has no predictive value.

Based on recent findings, NNDB has not witnessed high magnitude seismicity since its inception. However, very low magnitude earth tremors have sporadically occurred 10 times in the last three decades in Nigeria (Akpan and Yakubu, 2010). The epicentre and extent of the seismicities were badly interpreted on the evidence of insufficient seismic monitoring stations and poor comprehension. Adewole and Healy (2013) suggested a non-uniform SH_{max} direction from the analysis of good quality borehole breakouts, consistent with more than one source of stress in the region. If there are increasing seismic events in the neighbourhood of the Niger Delta Basin, particularly along the proximal continental margin, as reported by Ambraseys and Adams (1986) in Accra (Ghana) and Kribi (Cameroun); Figure 1(i), then the faults and other structures of the study area might be subjected to significant stresses in depth to some extent, which are likely to induce structural failures in the region. Our study is designed to help limit the impact of these potential failures in hydrocarbon exploration and mining.

3. Methodology

3.1 Data gathering and processing

Data were gathered from petroleum exploration sources to reconstruct in situ

conditions in the subsurface when faults are either stable or deemed liable to fail, and to quantify the key factor that may control the structural stability in the basin. Methods of estimating the essential data for fault stability calculations are presented with respect to their qualities, to better understand their relative effects on interpretations of stability models. Appropriate cautions have been applied in selecting these required data such that only model parameters of interest were resolved optimally.

3.2. Vertical stress

Vertical stress (S_v) is defined as the force applied vertically at a given depth by the weight of overlying rocks on a unit volume of rock at that depth (Jaeger and Cook, 1971; Engelder, 1993). The magnitude of the vertical stress for each modelled depth was estimated from density log data:

$$S_v = \sum_{Z}^{0} \rho(z)\, g\, \mathrm{dz} \quad (1)$$

where ρ is the density of the overlying rock column, g is the acceleration due to gravity, and z is the vertical depth.

S_v was estimated from 11 near vertical wells (Figure 4) located in the detailed study area. The clear separation of the S_v gradient profiles witnessed from a depth of 2.7 km indicates lateral variations of S_v gradients across wells. S_v gradients vary vertically with depth from 19 MPa/km (near surface; X_1) to 25.7 MPa/km (4 km; X_4), and laterally between wells, particularly at the top of high magnitude overpressures (3.5 km; Figure 3) from 23.6 MPa/km to 25.0 MPa/km (Figure 4; X_3). This result suggests that the S_v is not only depth-dependent but also driven by density variations reported in the basin (Adewole et al., 2016).

3.3. Pore fluid pressures

When sands and shales are in pressure equilibrium, as observed in the study area, pressures generally increase with depth (Webster et al., 2011). A higher pore fluid pressure in depth decreases the resistant of faults to sliding and increases the propensity of faults to failures (Streit and Hillis, 2004). In this paper, we have used pore fluid pressures information obtained from 87 wells drilled in the area (Figure 2) to assess the average magnitude of pore fluid pressures in the subsurface. Direct pore pressure measurements from these wells were plotted against their corresponding depths (Adewole et al., 2016), and the final result is presented in Figure 3. Apparently, the shallow depths (0-1.8 km) were missing good quality pressure data, which inevitably caused a deprivation of critical data set that might improve the accuracy of extrapolated pressure trends.

The idea of using a compilation of average pressures recorded from zones of normal pressure (2 km; Figure 3), top of rapid overpressures (3.5 km), and abnormal pressures (4 km) in the stability models has been founded on linking the distinctive subsurface conditions of a specific depth to some factors influencing the structural stability at that depth. We put this concept together to help understand the sensitivity of structures to failures in critical depths in the subsurface. In particular, the ability to determine beforehand the degree of stability provides a unique opportunity to ascertain with confidence the success rate of fault-bound hydrocarbon prospects, drilling of production-driven fluid injection wells, and storage of carbon dioxide.

3.4. Minimum horizontal stress (SH_{min}) magnitude

One of the most challenging tasks in a geomechanical analysis, which in most cases, seems unresolvable in a passive margin setting like the Niger Delta Basin, is to differentiate between the two components of horizontal stress; SH_{min} and SH_{max}. Breckels and Van Eekelen (1981, 1982), Bell (1990), and Reynolds et al. (2006) recommended the use of hydraulic fracturing (mini-frac or “fracking”) data and the lower

limit to Leak-Off Tests (LOT) in near vertical wells, if possible, for estimating the SH_{min} magnitude. However, Streit and Hillis (2004) and Reynolds et al. (2006) reported a significant amount of mini-frac data are more accurate for approximating SH_{min} than LOT data and Eaton (1969) method. Unfortunately, mini-frac data were not available in this study. Consequently, we a published SH_{min} data set (Figure 5, Adewole and Healy, 2013) for the modelling, constrained using Breckels and Van Eekelen method, patterned after the Gulf of Mexico, which has a significant quantity of mini-frac database. The accuracy of the empirical methods depends, to some extent, on the reliability of the input parameters, most especially, the Poisson ratio and pore fluid pressures. Out of the three methods at work in Figure 5, only Breckels and Van Eekelen fits the preferred LOT data quite well, although a clear parting from the normal trend is observed in the deep (marked by thick arrow), where the Breckels and Van Eekelen profile approaches 3.7 km, but the data show a small discrepancy as expected due to rapid overpressures. In general, combining the measurements of the stress data in the Breckels and Van Eekelen and LOT shows promising results as the reliable average magnitude of the SH_{min} values existing in the basin.

3.5. Maximum horizontal stress (SH_{max})

The SH_{max} value determined from the data in the study area is next in magnitude to the maximum principal stress (S_v), which suggests a predominant normal faulting regime in depth between 2 km to 4 km (Anderson, 1942; Adewole and Healy, 2013). An accurate estimation of SH_{max} requires the knowledge of pore fluid pressures, calibrated rock strength, S_v and SH_{min} data (Reynolds et al., 2006; Tingay, 2011).

If the normally preferred earthquake focal mechanism solution data are lacking in an area, then estimations of SH_{max} magnitude and direction may be unreliable (Zoback, 2010). However, SH_{max} can be evaluated from borehole image logs, Frictional Limit To Stress (FLTS), and Drilling Induced Tensile Fracture (DITF) data (Zoback and Healy,

1984). The selection of the appropriate method to use depends mainly on the tectonic history of the area, and the prevalent faulting regime. For instance, the FLTS data, beyond which faulting occurs, provide the upper limit estimate for the SH_{max} only in the strike-slip and reverse faulting regimes, where SH_{max} is the maximum principal stress (Anderson, 1942; Reynolds et al., 2006). The small differential stress between the two horizontal stress components (SH_{max} - SH_{min}), interpreted in the NNDB, is incompatible with the use of DITFs data if accessible. A reliable result is thus achieved when there is a significant horizontal differential stress, as found in the strike-slip faulting regime (Anderson, 1951; Moos and Zoback, 1990; Peska and Zoback, 1995; Adewole and Healy, 2013).

Apart from the difficulty compounded by the application of the preferred stress data discussed above, none of the data were available in this study. We thus reasoned out the well constrained lower limit of S_v data (Figure 5) to be the maximum possible range of SH_{max} magnitude attainable in the NNDB based on the closing up of the upper boundary of the SH_{max} magnitude with the lower limit of S_v (normal faulting regime, Anderson, 1942).

3.6. Maximum horizontal stress direction

As discussed earlier in the subsection 3.5, the preferred stress data, which unfortunately were not available for this study, are best suited to estimate the SH_{max} direction. Further reasons for not using other methods (tectonic activities, trend of folds, active reverse faults and regional stress patterns) can be found in Adewole and Healy (2013). The horizontal stress components show a geometric dependency on each other. The direction of SH_{max} is always at a right angle to the SH_{min}, thus an azimuthal constraint on one determines the other.

The SH_{max} directions have been obtained indirectly from the analyses of borehole breakouts in four arm caliper log data (Adewole and Healy, 2013), a product of

the dipmeter tool. Borehole breakouts are enlargements of the borehole wall when the circumferential stress in the borehole exceeds the intrinsic compressive rock strength. They are typically of an ellipsoidal shape (Bell and Gough, 1979, 1982; Reynolds et al., 2005). In near vertical wells, the direction of spalling of the wellbore fragments parallels the SH_{min} direction. A map view of the basinwide assessment of SH_{max} directions is shown in Figure 6. The square dot line in the lower right corner signifies apparent direction of volcanic cones alignment (interpreted on the map as a possible localised stress direction). The topographic data in the background are from the world stress map (Heidbach et al., 2008). It is clear from the map that no meaningful (uniform) SH_{max} direction can be derived, which perhaps indicates more than one single source of stress in the study area.

4. Calculation

4.1. Assessment of Fault Stability Indices

The appropriate calibration of the SI to the proper level of stability is the most interpretive phase in this stability quantification modelling. We now describe the fault SI used in this study.

4.1.1. Slip Tendency (T_s)

A slip is likely to occur on a surface when the resolved shear stress (τ) on that surface equals or exceeds the frictional resistance to sliding, which is proportional to the normal stress (σ_n) acting on the surface (Jaeger and Cook, 1979; Morris et al., 1996). Thus, slip tendency T_s is fairly well approximated by defined as

$$T_s = \tau / \sigma_n \qquad (2)$$

In this case, T_s depends on the in-situ stress field and the orientation of the fault surfaces. For instance, in a uniform stress field, some faults are relatively more favourably oriented for slip to take place than others. Furthermore, the predisposition of a surface to slip depends largely on its cohesive strength and the coefficient of static friction (μ). By implication, μ is the value of T_s that will cause a slip on a cohesionless surface. T_s' is the normalised slip tendency defined as T_s / max(T_s).

In this paper, the scale of T_s' ranges from 0 (low risk) to 1 (high risk). Several mechanisms can combine to produce substantial changes in the stability of a structure. It is therefore difficult to understand and quantify in real terms the required magnitude of shear stress that is likely to cause a significant structural failure. A fault surface with T_s value ≥ 0.6 (Byerlee, 1978) is considered in this study to be in an appropriate condition for slip to take place. Faults that are close to the ideal orientation for slips are invariably connected with zones of high fracture density and enhanced permeability (Ferrill et al., 1999). However, after a failure, porosities of fault zones, particularly in sands and shales, are considerably reduced or sometimes can be enhanced depending on the rock strength and degree of compaction (Handin et al., 1963; Knipe, 1986; Lucas and Moore, 1986; Hooper, 1991).

4.1.2. Dilation Tendency (T_d)

The studies of Ferrill et al. (1999), as well as some previous works (Carlsson and Olsson, 1979), indicate that T_d is a measure of reopening of a fault or fracture for the passage of a fluid, and is defined as:

$$T_d = \sigma_1 - \sigma_n \ / \sigma_1 - \sigma_3 \qquad (3)$$

where σ_1 is the maximum principal compressive stress, and σ_3 is the minimum principal compressive stress. The ability of a fault to allow the fluid to pass invariably depends on the size of the aperture after dilation.

The T_d of a fault is chiefly measured by the effective normal stress (σ_n - P_p) acting upon it, which according to Ferrill et al. (1999) is determined by the lithostatic, tectonic stresses, pore fluid pressure, and the relative orientation of the fault plane to the direction of stresses. For instance, a fault that is oriented perpendicular to σ_1 may tend to close, and therefore have a minimal aperture, which reduces the permeability of the fault zone to low values (Carlsson and Olsson, 1979). In a situation whereby the magnitude of the σ_1 is strong enough to close a fault in a very favourable orientation to the stress field, the fault will exhibit a low T_d and may not be conductive to fluid. On the contrary, the fluid permeability may not be affected (or a little effect if any) if the magnitude of the maximum principal stress is not strong enough to cause a reduction in fault apertures. The scale of the T_d values in this study has been graded from 0 (low risk) to 1 (high risk).

4.1.3. Fracture Stability (F_s)

The stability of a fracture is estimated by determining the increase in pore fluid pressures required to push a fault into a shear or extensional. In a normal cohesionless rock, the intrinsic shear strength (C) of a fault is presumed 0. The τ inducing slip within the fault failure envelope is of the form (Hubbert and Rubey, 1959; Streit and Hillis, 2004)

$$\tau = C + \mu (\sigma_n - P_p) \quad (4)$$

Thus, the Fracture Stability, F_s, defined as the pore fluid pressure required to induce slip when C = 0 can be written as

$$F_s = \sigma_n - (\tau/\mu) \quad (5)$$

It is vital to correctly calculate pore fluid pressure for better understanding of its influence, particularly in an area where the presence of significant overpressures in depth has been reported such as the NNDB (Adewole et al., 2016). Generally, higher pore fluid pressures decrease the resistance of faults to sliding, but invariably subject to the pressure magnitude, and some crucial parameters defining the shear stress of the faults under failure conditions (equation 4). An increase in pore fluid pressure may generate new fractures instead of reactivating the existing ones (Streit and Hillis, 2004). Pore fluid pressure has an ability to change the hydraulic seal of geological faults and modify the flow capacity of natural fractures considerably (Sibson, 1996). Other factors controlling the magnitude of increasing pore fluid pressure reaching the failure envelope are: (i) the orientation of the fault plane to stress field; (ii) differential stress (σ_1 - σ_3); (iii) the magnitudes of tensile & cohesive strengths. These factors also determine the resulting mode of failure; shear, extensional and extensional-shear. It is possible for a slight increase in the pore fluid pressure to lead to any of the mode of failures under favourable conditions. The fault that has a high risk of failure will exhibit low F_s.

4.2. Geomechanical modelling

Fault stability modelling depends on several assumptions. Because of the diversity in rock materials, two scenarios were considered: scenario one typifies a cohesive rock condition where the materials constituting the fault surfaces characterise a high coefficient of internal friction (μ_i) and a high cohesion (C_i), whereas scenario two exemplifies a relatively less cohesive condition with a lower μ_i, and a lower C_i. The SI has bee estimated using fault stability analysis software (Badley, 2012). The scenarios

represent different brittle shear fracturing conditions of rocks based on their textural properties and diagenetic conditions.

Although in many stratigraphic settings, particularly those that are rich in smectite at shallow depth (< 2.5 km), scenario two is favourably disposed towards instability, but becomes less likely with increasing depth due to the preferential mixture and consolidation of sediments. However, we chose to use scenario one here for the models because the appropriate stress and pore fluid pressure conditions that were likely to compromise the stability of faults under high strength brittle shear fracturing conditions were targeted. This was conceptualised on the reason of uncertainty remains regarding the impact of fluid and sediment mixtures in defining sediment properties. For instance, as discussed in section 2, the modelled faults were situated within the paralic sequence (contains mixed continental sand, brackish water and marine deposits), overlaid by continental sands and gravel (Weber, 1971). Existences of high fluid saturations within the sediment pore spaces have been demonstrated to significantly modify the physical properties of sediments (shear strength, volume changes and permeability; Waite et al., 2009). Other advantages of using scenario one are: (i) while maintaining the minimum number of models parameters, it allowed us to model from the shallow to the deep; (ii) to obtain a very distinctive interpretations from the continuous change in the SH_{max} direction away from the basinwide estimate (Figure 6).

We have modelled fault segments from four major growth faults: (a) anti1; (b) anti2; (c) Fa1; and (d) Fa2, interpreted from the 3D seismic data as shown in Figure 7. The coloured contour lines on the fault surfaces represent relative positions of the interpreted layers on the fault blocks. The apparent increase in the contour space with depth between a pair of contours (upthrow and downthrow) of the same colour is suggestive of an increase in the fault throw with depth in the region. The dilation value at a fault to a pole position on the stereonet indicates the degree of dilation of the fault segment at that point. The four horizon-based faults interpreted from the seismic data

were plotted on the rose diagram and histogram (Figure 8) to show directions and relative distributions of the fault strikes respectively. However, we considered only fault segments related to three horizons (shallow, intermediate and deep) characterising apparent deformations in depth.

The stress and pressure data constrained in the NNDB in previous studies (Adewole and Healy, 2013; Adewole et al., 2016) at predetermined depths: (i) shallow (2 km); (ii) intermediate (3.5 km); and (iii) deep (4 km), built on a pressure history of the study area were adopted as parts of the model parameters (Table 1). The fault SI has been evaluated in each of the SH_{max} directions (rotated by 15^o interval) from 0^o to 90^o. The relative positions of the fault segments on equal angle stereographic projections of the fault SI were used to determine dips and related azimuths of fault segments that are susceptible to failure as illustrated in Figures 7(B).

Table 1

The depth parameters for each faulting regime within the proposed stability models

Faulting region	Depth (m)	SH_{max} (MPa)	SH_{min} (MPa)	S_v (MPa)	HP (MPa)	P_p (MPa)	Gradient (MPa/km)				
							SH_{max}	SH_{min}	S_v	HP	P_p
Normal	2,000	42	29	49	22	23	0.021	0.015	0.02	0.011	0.012
	3,500	76	64	85	36	45	0.022	0.018	0.02	0.010	0.013
	4,000	88	79	102	42	59	0.022	0.020	0.02	0.011	0.015
Pseudo-Strike-slip	2,000	49	26	31	22	23	0.025	0.013	0.01	0.011	0.012
	3,500	85	45	53	36	45	0.024	0.013	0.01	0.010	0.013
	4,000	102	54	64	42	59	0.026	0.013	0.01	0.011	0.015
Pseudo-thrust	2,000	49	31	26	22	23	0.025	0.015	0.01	0.011	0.012
	3,500	85	53	45	36	45	0.024	0.015	0.01	0.010	0.013
	4,000	102	64	54	42	59	0.026	0.016	0.01	0.011	0.015

The SH_{max} direction was rotated at intervals of 15^o from 0^o to 90^o in each depth, and the orientation of SH_{min} was set at 90^o to the direction of SH_{max}. Parameters for defining a failure envelope on the Mohr diagram are: (i) Scenario one: μ = 0.45, C_F = 0.5 MPa. (ii) Scenario two: μ = 0.33, C_F = 2 MPa (Dewhurst and Jones, 2002; Dewhurst and Hennig, 2003). The average stress ratios in the normal faulting are 34% SH_{max}, 39% S_v, and 27% SH_{min}. Gradient = stress magnitude/depth; HP = Hydrostatic pressure; P_p = Pore fluid pressure; C_F = Coulomb failure criterion

The pseudo-strike-slip and pseudo-thrust faulting models are to cater for a possible future change in the dominant normal faulting regime. For this to occur in this basin, the tectonic process must be sufficient to redistribute the magnitude of the stress

components in a way that the SH_{max} *d*isplaces S_v as the principal stress. A clear evidence of this sort of stress-transposing mechanism can only materialise on a regional scale (hundreds to thousands of square kilometres) of continuous lithostratigraphic units. An example can be found in the 1995 Kobe earthquake, Japan, where the original stress vectors (magnitudes and directions) of the rocks were modified by an earthquake fault slip. In this case, the full stress tensor of the affected region was vectorially altered after the earthquake (Yamashita et al., 2004). This reinforces the need for a continuous measurement of stress attributes, especially in a seismically active region to confirm the stress direction and a possible change in the faulting regime.

Much more efforts have been made in broadening the understanding of the pattern of developments of seismicities related to solid mineral mining activities, particularly the initiation of multiphase mechanisms leading to creations of new faults or reactivations of existing ones. For instance, the mining of a coal seam underground may auspiciously create conditions for the development of massive geologic structures (faults, subsidence columns, coal tunnels and gobs) as occurred in the coalfield located in the eastern China (Jingbin et al., 2016). The localised stress equilibrium is disposed to modification if the shear and tensile stresses of host rocks increase as deformation processes of the stratigraphic units heighten. It happens when the overburden rocks above the area previously occupied by the mined coal seam lose support, causing the underlying layers to deform, move and ultimately collapse. In a different process, intensive hydrocarbon production activities at times necessitate the use of fluid injection wells to boost production. This practice has implications for ramping up stress magnitudes and pressures in the subsurface. Multiple faults created in this way will certainly have distinct geometries from the existing ones.

The average stress ratios constrained in the study area are given in Table 1; 34% SH_{max}, 39% S_v, and 27% SH_{min}. In order to provide the required stress magnitudes

and create appropriate conditions for pseudo-faulting regimes, especially to suit the typically low seismicity region, we have implemented the average ratios of the stress components (46.5% SH_{max}, 29% S_v, and 24.5% SH_{min}) in two prominent strike-slip faulting basins; Cooper-Eromanga, Australia (47% SH_{max}, 28% S_v, and 25% SH_{min}; Reynolds et al., 2006), and St. Lawrence Lowlands, Canada (46% SH_{max}, 30% S_v, and 24% SH_{min}; Konstantinovskaya et al., 2012). The selection of these areas was based on their geologic locations within high stress environments with substantial magnitudes for the full stress tensor, harmonising Anderson principles (Anderson, 1942, 1951). The minimal differential stress ratios in both basins can be easily interpreted in terms of variations in the source and intensity of the stresses. In the two basins adapted here, the differential stresses against the SH_{max} (SH_{max}-S_v and SH_{max}-SH_{min}) are apparently larger than those of the study area as expected in high seismicity regions. If a basin is highly overpressured as the case in the study area, the rock stresses have tendency to change in such a way that small differences will exist between the magnitudes of the three principal stresses (S_v, SH_{max} and SH_{min}, Zoback, 2010).

The direct integration of the estimated S_v data from the study area (initially conceived at the earlier stage of this work) into the pseudo-faulting analyses has significant difficulties and unreliable interpretations with the results of the average stress ratios method. The fundamental difficulty is that the outcome of the derived SH_{max} appears spurious, and could not be favourably matched with any known active seismicity basins. Although it was observed that the S_v data were generally high, because the area of study, in comparison to other basins of similar depositional and stratigraphic settings, has not witnessed significant uplift or exhumation since deposition (Adewole et al., 2016). For instance at 4 km depth, giving the S_v value of 102 MPa (Table 1), working out the SH_{max} by applying the average stress ratios (pseudo-faulting analyses) will scale up the value to 269 MPa, which is exceedingly out of the range of proportionate values desired (< 205 MPa; Reynolds et al., 2006). In contrast,

at the same depth in the seismically active Cooper-Eromanga Basins, the SH_{max} value of 108 MPa and gradient of 27 MPa/km were evaluated by Reynolds et al. (2006). Thus, the SH_{max} may be overdetermined in depth, which is likely to undermine the model predictions.

The estimated S_v data were adopted for the maximum principal stress (SH_{max}) in the pseudo-faulting analyses. Then, we adjusted the average stress ratios of the strike-slip faulting system to reflect a true thrust faulting as presented in Table 1. This was particularly simple because the relative magnitudes of the stress components were cross-checked against the faulting regime to stress magnitudes relationships reported by Anderson (1942, 1951), which are: (i) normal faulting system ($S_v > SH_{max} > SH_{min}$); (ii) strike-slip faulting ($SH_{max} > S_v > SH_{min}$); (iii) thrust faulting ($SH_{max} > SH_{min} > S_v$).

5. Results and discussions

In this study, no model can be regarded as very well established, even though ample efforts have been made in identifying and evaluating the variables controlling the general stability of faults in the subsurface. It is particulary difficult to model tectonic processes in pseudo-faulting conditions. In the normal faulting regime, because the SH_{max} could not be determined directly, the adapted data from the lower bound of S_v may be insufficient to produce reliable results. The basic assumptions might have limitations with consequences that are prone to misinterpretation. It must be recognised that the fallouts of any wrong computation in this way can compromise results of the assessment of fault stability.

The near horizontal strike directions of all the interpreted faults, as illustrated in Figure 8, demonstrate at least the degree of the homogeneity in the faulting system in depth, which can be mechanically linked to the similar thrust (gravitational slumping heightened by compaction as discussed in section 2; Weber, 1971) on the faulting

mechanisms. The mean fault strike direction is likely to facilitate the movement of a directional high stress to effect structural failures that are capable of traversing less tortuously from the deep to the surface through the faults. It shows the need to accurately constrain stress magnitude and direction in the subsurface to guarantee the stability of failure-prone downhole tools and structures.

5.1. Normal faulting regime

The results of the models are strongly dependent on the uncertainties of the available input data sets earlier mentioned. Overcoming these challenges in the data is a difficult task. Some new strategies are needed to handle them in a resourceful manner. The model results are grouped as follows:

(i) 2.0 km depth: All the fault segments show a very high stability for 0^o, 15^o and 30^o models. However, a significant number of them indicate a very high likelihood of dilation, slip (Figure 9) and instability (Figure 10) for SH_{max} direction models above 30^o, became severe at 60^o and approached a critical limit at 90^o. The overall indication of fault stability in this level is presented in Table 2.

Table 2

The result of the fault stability interpreted from the SI in different tectonic faulting regimes

SH_{max} direction	SI	Normal faulting			Pseudo-strike-slip faulting			Pseudo-thrust faulting		
		2 km	3.5 km	4 km	2 km	3.5 km	4 km	2 km	3.5 km	4 km
0-30^o	T_d	H	H	H	H	H	H	H	H	H
	T_s	H	H	H	H	H	H	H	H	H
	F_s	H	H	H	H	H	H	H	H	H
30-60^o	T_d	M	M	L	M	L	M	M	M	M
	T_s	M	M	M	M	M	M	M	M	M
	F_s	M	M	M	M	M	M	M	M	M
60-90^o	T_d	L	L	L	L	L	L	L	L	L
	T_s	L	L	L	L	L	L	L	L	L
	F_s	L	L	M	M	M	L	L	L	L

H = High stability, M = Mild stability; L = Low stability. The models have been grouped based on close similarities of the results, which are indicative measurements of fault stability in the study area. The criteria of SI for determining the degree of stability (L, M and H) were based on the level of disparity of the

SI against the base values of its elements (T_s = 0.6, T_d = 0.5 and F_s = 0.8 MPa). For instance, a high stability interpretation implies SI elements with T_s < 0.6, T_d < 0.5 and F_s > 0.8 MPa.

(ii) 3.5 km depth: The faults indicate low to medium T_s, and more disposed to a higher dilation and slip, and lower stability from 30^o to 90^o models. Normally, if the two scenarios are subjected to similar conditions (stress field and pressures), some of the SI elements may show near similar strength indicators, which at times may be demanding to effectively construe. For example, the T_d effects displayed on the stereogram in the scenario one model; Figure 11(A), are apparently similar to those of scenario two; Figure 11(B). In contrary, the fracture stability tested with a low pressure of 16 MPa resolved the differences, which could not easily observed on the stereograms as shown on the Mohr circles (Figure 11). The striking differences in the positions of Coulomb failure lines (Mohr circles) are attributed to the differential shear strength of the materials. In this case, for a fault to attain a substantial level of instability in the scenario one requires relatively higher stress and pore fluid pressure than the scenario two. More vitally here, it demonstrates the need for the full measurement of all the SI elements for a proper assessment of the stability in the subsurface.

In addition, this depth marks the onset of rapid overpressures in the basin. Pore fluid pressures vary laterally between wells and vertically with depth (Adewole et al., 2016). Pressures above hydrostatic are capable of draining vertically and hastening failures of fault seals as documented in other deltaic basins similar to the Niger Delta Basin around the world, such as the Baram delta province, Brunei (Tingay et al., 2003, 2009), and Taranaki Basin, New Zealand (Webster et al., 2011). The assessment of hydrostatic pressure and overpressure-based models shows that the average F_s value for the hydrostatic pressure-based condition in all the models (from 0^o to 90^o) is 1.2 MPa, which is high enough to make all the faults stable (>0.8 MPa), whereas the F_s value for the overpressure-based models is lower (0.55 MPa), suggesting a possible reduction of the fault strength (< 0.8 MPa) by high magnitude overpressures.

The example presented in Figure 12 principally shows the influence of increasing pore pressures on the fracture stability (normal faulting regime) at the same depth. The model results of the average pressure measured from wells (45 MPa), as illustrated in (B), were compared with those of the simulated pore pressures values 36 MPa (A), 50 MPa (C), and 65 MPa (D); Figure 12. The decreasing fracture stability from (A) to (D), and the systematic shift in positions of the Mohr circles from P_o; right of the Coulomb failure line in (A), to P_1; left of the Coulomb failure line in (D), are consistent with the increasing pressures from (A) to (D). Thus, at higher pore fluid pressures (≥ 50 MPa), the faults are predisposed to failures. The pore fluid pressures that induce new fractures are usually greater than the maximum sustainable fluid pressure on faults (Streit and Hillis, 2004).

(iii) 4 km depth: The faults generally display high T_d values and moderate F_s from 30^o to 90^o models, whereas the T_s is averagely low to moderate in all the models. This observation is consistent with the level of irregularities associated with the evaluation of fault stability at this depth, partly due to the variation in the effects of diagenetic processes in depths, which could not be easily quantified.

5.2. Pseudo-strike-slip faulting regime

(i) 2 km depth: T_d around the faults increases gently in the 30^o and 45^o models, but becomes rapid from 60^o to 90^o. However, F_s exhibits mild values from 30^o to 90^o models. This result does not conform to the very high stability from 0^o to 30^o models and a low to mild stability from 45^o to 90^o observed in the normal faulting regime given the same conditions (Table 1). It suggests some instances may occur where a change in the faulting regime is likely to influence the fault stability.

(ii) 3.5 km depth: T_d displays remarkably low stability from 30^o to 90^o models, whereas the F_s and T_s indicate mild to low stability in the same models. The reason is

largely due to the pull down effect of rapid overpressures at this depth, which is capable of reducing effective stress.

(iii) 4 km depth: Mild to low T_d stability was also observed at this depth from 30^o to 90^o (Figure 13). The F_s and T_s also correspondingly indicate similar stability characteristics in all models, as witnessed at 3.5 km depth. This effect has been largely driven by model parameters, particularly the stress magnitudes. Thus, linking the interpretation to the general influence on the state of fault stability at deep level is difficult to quantify with this technique because of their full range of uncertainty.

Because the majority of the faults virtually strikes averagely east-west direction (Figure 8), the fault apertures are likely to close up if the SH_{max} direction is rotated to 0^o and 15^o, since these directions are in near perpendicular positions to the faults. Thus, the faults show a very high stability from 0^o and 15^o models.

5.3. Pseudo-thrust faulting regime

(i) 2 km depth: High T_d stability was observed from 0^o to 30^o models. The increasing T_d values evaluated from 30^o to 90^o models show a remarkable agreement with the results of the normal and strike-slip faulting regimes. On the contrary, F_s decreases very fast from 30^o to 90^o models, which is only consistent with the result of the normal faulting regime, but differs slightly from that of the pseudo-strike-slip, that largely shows a low to moderate stability in all models.

(ii) 3.5 km depth: The faults show a very high T_d and decreasing F_s from 30^o to 90^o models. These observations correspond with results of the normal and pseudo-strike-slip faulting regimes. In this context, the consistency of the model results across all the faulting regimes indicates that overpressure effects on the fault stability are independent of the regional faulting regime. This allows the influence of pressure to be evaluated with a single-step procedure directly from all the models, but the necessity of

computing the exact pressure magnitude in depths that is likely to cause a fault to absolutely fail along its plane poses some challenges across the faulting regimes.

(iii) 4 km depth: It can be observed that all the models at this depth correlate well with those of other faulting regimes. For instance, the increasing T_d detected here from 30^o to 90^o models corresponds with the decreasing F_s within the same range in all the faulting regimes (Figure 14).

The final decision will concern how variability and uncertainty in the model parameters (Table 1) are likely to affect the overall interpretations (Table 2). These sort of parameter-definition problems, particularly at deep levels, constitute a difficult task in assessments of the model results. For instance, the quality of the stress data invariably affects the model results. Because of the optimum superiority of data sets, Nelson et al. (2006) preferentially suggested the use of the earthquake focal mechanism solution to define SH_{max} data in a thrust-faulting regime instead of the conventional well data.

For better interpretation of all the fault models, the fault dips and their corresponding azimuths, which were computed to most likely fail based on the afore mentioned criteria of the SI for unstable faults, are presented on histograms (A) and rose plots (B) respectively (Figure 15). The simple technique used here highlighted the lower limit of the azimuth pertaining to unstable fault segments on the stereograms, and assumed it to be the least failure direction. The evaluations of the models based on the defined failure criteria of the SI and at least 20% of the sampled data (Figure 15) demonstrate that some of the key faults in the normal faulting regime (50^o - 60^o and 80^o - 90^o dips and 100^o - 110^o azimuths), pseudo-strike-slip (10^o - 20^o and 80^o - 90^o dips, and 100^o - 110^o azimuths), and pseudo-thrust (10^o - 20^o dips and 100^o - 110^o, and 210^o - 220^o azimuths) present the greatest risk on the base of probability under most favourable conditions (pressures and stresses). The degree of probability indeed, in most cases, depends on the quality and reliability of the input data sets.

5.4. Implication for hydrocarbon prospects and increased seismicities

The interpretations of the model results in the three faulting regimes point out that the direction of the maximum horizontal stress to the subsurface faults played a key role in the assessment of fault stability in the subsurface. The use of SI in determining which networks of fractures have tendencies to be stable and unstable can also contribute to the fulfilment of the need to carry out a predrill assessment of hydrocarbon prospects, directly mapped from integrated geophysical and geological data. This is most essential when maturing prospective hydrocarbon levels to identify the effectiveness of structural and stratigraphic traps, and safeguard the drilling of unproductive and unsafe wells.

In active producing fields, fluid injection wells and long years of hydrocarbon productions within the same fields may create favourable setting for a high stress build-up in the reservoirs, and break fault seals, thus enhancing the likelihoods of the reactivation and conductivity of faults for fluid migration. Pressurised fluids migrating along weak or unstable faults are capable of travelling long distance, and at times under ideal conditions, displacing prospective gas accumulated at the top of reservoirs. Then, as a result overpressures, the displaced gas beneath becomes virtually inaccessible to the explorationists

Likewise, using the result of this study to explain the reason for the occurrence of over 30 earth tremors, majorly felt in the middle and southern Nigeria in the past eight decades (Adewole and Healy, 2013), and combining it with the recent spate of over 10 tremors in the last two years, particularly the ones that happened within areas of intensive hydrocarbon exploration and solid minerals mining activities (displayed as ET1 and ET2, Figure 1): (i) ET1, south west, Nigeria (Lagos and Saki) and (ii) ET2, south, Nigeria (Yenagoa, Ahoada, Igbogene, Mbiama, and Ikarama). The high use of explosives and injection of fluids for mining purposes provide ideal conditions in the subsurface for far-reaching structural failures to occur. The increasing rate of the

incident and intensity of the earth tremors in these selected areas allow us to determine not only that some faults might have been reactivated (possibly the close by rifted continental crust faults), but also suggest that the tremors have dynamic propensities to develop into separate extremities (high magnitude earthquakes) if the increasing stress and pressure ascribed to the mineral exploration activities are not reduced or possibly discontinued, particularly in the compressive region of the shallow and deep offshore (Figure 1).

It is challenging to simply attribute the transformation of the faulting regime in an area to after-effects of mineral exploitation activities without factoring in impacts by regional tectonic activities, and the need to precisely estimate vectorial properties of induced stresses and the type of fault displacements, which in this case, is the expected structural significance. More importantly, it is demanding to successfully constrain these parameters from the conventional low resolution data (seismic or well), which are usually reasoned, for this purpose, to have limited well coverage, and perhaps a less affected and discontinuous mining area. In some cases, the data may even be too scanty to capture the details and changeability of faulting regimes.

We believe our method in this paper will have significant applications in determining appropriate geomechanical properties that are very crucial for hydrocarbon field development, reservoir production and facility constructions.

6. Conclusions

We have used fault SI to model the stability of faults interpreted from the 3D seismic data using constrained stress and pore fluid pressure data measured directly from neighbouring wells. We used a set of alternative SH_{max} directions to account for possible changes in the stress directions and faulting regimes by tectonic and non-tectonic forces.

Faults that show particular characteristics of SI (high T_s, low F_s, and high T_d values) are deemed to be within risky zones subject to certain favourable conditions (stress, pressure, and ideal orientations for failure). Although many models exhibit similar results in depths, but some independent results were observed indicating a possibility of an anisotropic situation across faulting regimes. Some models that apparently show consistent results in different faulting regimes provide clear evidence to support our proposition here that the maximum principal stress and pore fluid pressure are crucial determinants of stability measurements in subsurface structures, which have to be well constrained to improve the record of reliability of the results. Conversely, the diversity of a few model results reinforces the need to exercise great caution when predicting fault failures across faulting regimes. Influences of overpressures on the general stability of faults appear to be independent of the prevalent faulting regime. The dip of a fault is also independent of the principal SH_{max} direction. In the study area, the average east-west strike direction of the faults is consistent with the high stability observed in the 0^o and 15^o SH_{max} models. For this reason, if the SH_{max} direction changes to at least 45^o, nearly all the faults will be potentially liable to failure given other enabling factors.

We believe that further works on our proposed techniques will offer the potential to lay the groundwork for additional reasonable predictions of the structural stability throughout the hydrocarbon trapping-forecast, superinduced seismicity from mining activities, and the critical decision making processes. Pressure data are available in the basin, but little has been published in the way of stress data, particularly the full horizontal stress. Future works will focus on integrating solutions to stress data uncertainty in depths into the models. Because SI alone are not a definitive indicator of fault stability, particularly in the field of hydrocarbon exploration, upgraded integrations with other geologic data sets are crucial next steps after modelling. Generally, as we improve our in-depth understanding of stress and pressure data, we would expect a

wide range of applications. We also anticipate many new developments in the evaluations of structural failures in different tectonic regimes in the years to come.

Acknowledgement

Some of the data used in this study have been published by Adewole and Healy (2013), among others. The authors especially acknowledge Professor David Macdonald for his invaluable contributions and co-supervising the research project. Our thanks are due to the Department of Petroleum Resources (DPR) and anonymous oil companies in Nigeria for giving permission to access some of the data for this study. E. O. A. also thanks Judith Christie, Clare Bond and other members of the Department of Geology and Petroleum Geology, University of Aberdeen, Aberdeen. We greatly appreciate the editor, and two anonymous reviewers for their critical assessments and vital comments, which tremendously improved the overall quality of the manuscript. Continuous supports on TrapTester software provided by Badleys, UK on the estimation of SI are much appreciated. The authors gratefully acknowledge the management of PCS Earth Techs Ltd (Port Harcourt), Halliburton (Seisworks, ZMap and Stratworks), Kingdom, Rocdoc (Ikon science), EZ-ROSE, and CGG Veritas (Elog, Strata and AVO) for provisions of software and assistances.

References

Adewole, E.O., Healy, D., 2013. Quantification of in-situ stress in Niger Delta Basin, Nigeria. Global Science & Technology Forum (GSTF) Journal of Engineering Technology (JET) 2(3), 30-38.

Adewole, E.O., Macdonald, D.I.M., Healy, D., 2016. Estimating density and vertical stress magnitudes using hydrocarbon exploration data in the onshore Northern Niger Delta Basin, Nigeria: Implication for overpressure prediction. J. Afr. Earth Sci. 123, 294-308.

Akpan, O.U., Yakubu, T.A., 2010. A review of earthquake occurrences and observations in Nigeria. Earth science 23, 289-294.

Ambraseys, N.N., Adams, R.D., 1986. Seismicity of West Africa. Annales de Geophysique 4, 679-702.

Anderson, E.M., 1951. The Dynamics of Faulting and Dyke Formation with Applications to Britain. Oliver and Boyd, Edinburgh.

Anderson, E.M., 1942. The Dynamics of Faulting and Dyke Formation. Oliver and Boyd, Edinburgh and London.

Avbovbo, A.A., 1978. Tertiary lithostratigraphy of Niger Delta. America Association of Petroleum Geologist Bulletin 62, 295-300.

Badley Geoscience Ltd., 2012. Work flow advisor manual for structural, seismic interpretation, structural modelling and fault seal. Traptester 6.0 manual.

Bell, J.S., 1990. The stress regime of the Scotian Shelf offshore eastern Canada to 6 kilometres depth and implications for rock mechanics and hydrocarbon migration, in Maury, V. (Ed.), Rock at Great Depth, Balkema, Rotterdam, pp. 1243-1265.
Bell, J.S., Gough, D.I., 1982. The use of borehole breakouts in the study of crustal stress. United States Geological Survey Open File Report 82-1075, 539-557.
Bell, J.S., Gough, D.I., 1979. Northeast-southwest compressive stress in Alberta-Evidence from oil wells. Earth and Planetary Science Letters 45, 475-482.
Breckels, I.M., Van Eekelen, H.A.M., 1982. Relationship between horizontal stress and depth in sedimentary basins. Journal of Petroleum Technology 34, 2191-2198.
Breckels, I.M., Van Eekelen, H.A.M., 1981. Relationship between horizontal stress and depth in sedimentary basins.
Burke, K., 1972. Longshore drift, submarine canyons and submarine fans in development of Niger delta. American Association of Petroleum Geologists Bulletin 56, 1975-1983.
Byerlee, J.D., 1978. Friction of rocks. Pure and Applied Geophysics 116, 615-626.
Calvez, L., Joel, H., Bruno, V., 2002. Physical modelling of normal faults and graben relays above salt: A qualitative and quantitative analysis. Gulf Coast Association of Geological societies transactions 52.
Carlsson, A., Olsson, T., 1979. Hydraulic conductivity and its stress dependence. , 249-259.
Davies, R.K., Crawford, M., Dula, W.F., Cole, M.J., Dorn, G.A., 1997. Outcrop interpretation of seismic scale faults in S. Oregon: description of structural styles and evaluation of sub-surface interpretation methods. The Leading Edge 16, 1135-1140.
Dewhurst, N.D., Hennig, A.L., 2003. Geomechanical properties related to top seal leakage in the Carnarvon Basin, Northwest Shelf, Australia. Petroleum Geoscience 9, 255-263.
Dewhurst, N.D., Jones, R.M., 2002. Geomechanical, microstructural, and petrophysical evolution in experimentally reactivated cataclasites: Applications to fault seal prediction. American Association of Petroleum Geologists Bulletin 86, 1383-1405.
Doust, H., Omatsola, E., 1990. Niger Delta, in Edwards, J.D. (Ed.), Divergent/passive Margin Basins, AAPG Memoir 48 ed. American Association of Petroleum Geologists, Tulsa, pp. 73-89.
Eaton, B.A., 1969. Fracture gradient prediction and its application in oilfield operations. Journal of Petroleum Technology 246, 1353-1360.
Engelder, T., 1993. Stress Regimes in the Lithosphere. Princeton University press, Princeton.
Evamy, B.D., Haremboure, J., Kamerling, P., Knaap, W.A., Molloy, F.A., Rowlands, P.H., 1978. Hydrocarbon habitat of tertiary Niger delta. American Association of Petroleum Geologists Bulletin 62, 1-39.
Ferrill, D.A., Winterle, J., Wittmeyer, G., Sims, D., Colton, S., Armstrong, A., 1999. Stressed Rock Strains Groundwater at Yucca Mountain, Nevada. GSA Today 9, 1-8.
GeoMapApp., 2014. Maps: Africa drainage basins, world shorelines, geologic feature data table, country boundaries and topography and bathymetry images. 2014.
Handin, J., Hager Jr., R.V., Friedman, M., Feather, J.N., 1963. Experimental deformation of sedimentary rocks under confining pressure. American Association of Petroleum Geologists Bulletin 47, 717-755.
Heidbach, O., Tingay, M., Barth, A., Reinecker, J., Kurfeß, D., Müller, B., 2008. The World Stress Map database release 2008. doi:10.1594/GFZ.WSM.Rel2008 .
Hooper, E.C., 1991. Fluid migration along growth faults in compacting sediments. Journal of Petroleum Geology 14, 161-180.
Hosper, J., 1971. The geology of the Niger Delta area, in Delany, F.M. (Ed.), The Geology of the East Atlantic Continental Margin, Report No.70/16 ed. Institute of Geological Sciences, pp. 121-142.
Hospers, J., 1965. Gravity field and structure of the Niger Delta, Nigeria, West Africa. Geological Society of America Bulletin 76, 407-422.
Hubert, M.K., Rubey, W.W., 1959. Role of fluid pressure in mechanics of overthrust faulting. Geological Society of America Bulletin 70, 115-166.
Jaeger, J.C., Cook, G.W., 1979. Fundamentals of Rock Mechanics , 3rd ed. Chapman and Hall, London.
Jaeger, J.C., Cook, N.G.W., 1971. Fundamentals of Rock Mechanics. Chapman and Hall, London.
Jingbin, C., Zhonghong, W., Ping, C., Quanhu, L., Chen, X., 2016. The application of seismic attribute analysis technique in coal field exploration. Interpretation 4, SB13-SB21.
Knipe, R.J., 1986. Faulting mechanisms in slope sediments: Examples from DSDP cores, in Moore, J.C. (Ed.), Structural Fabrics in DSDP Cores from Forearcs, 166 ed. Geological Society of America Journal, pp. 89-103.
Konstantinovskaya, E., Malo, M., Castillo, D.A., 2012. Present-day stress analysis of the St. Lawrence Lowlands sedimentary basin (Canada) and implications for caprock integrity during CO2 injection operations. Tectonophysics 518-521, 119-137.
Lucas, S.E., Moore, J.C., 1986. Cataclastic deformation in accretionary wedges: DSDP Leg 66, southern Mexico, and on-land examples from Barbados and Kodiak Islands, in Moore, J.C. (Ed.), Structural Fabrics in DSDP Cores from Forearcs, 166 ed. Geological Society America Memoir, pp. 89-103.
Matthai, S.K., Aydin, A., Pollard, D.D., 1996. Pressure and fluid-flow response to production from reservoirs bounded by faults with relay structures.

Merki, P.J., 1972. Structural geology of the Cenozoic Niger delta. , 635-646.
Moos, D., Zoback, M.D., 1990. Utilization of observations of well bore failure to constrain the orientation and magnitude of crustal stresses: application to continental, deep sea drilling project and ocean drilling program boreholes. Journal of Geophysical Research 95, 9305-9325.
Morley, C.K., Nelson, T.P., Munn, S.G., 1990. Transfer zones in the East African rift system and their relevance to hydrocarbon exploration in rifts. American Association of Petroleum Geologists Bulletin 74, 1234-1253.
Morris, A.P., Ferrill, D.A., Henderson, D.B., 1996. Slip-tendency analysis and fault reactivation. Geology 24, 275-278.
Nelson, E., Hillis, R., Sandiford, M., Reynolds, S., Mildren, S., 2006. Present-day state-of-stress of southeast Australia. Australian Petroleum Production and Exploration Association Journal 46, 283-306.
Peska, P., Zoback, M.D., 1995. Compressive and tensile failure of inclined well bores and determination of in situ and rock strength. Journal of Geophysical Research 100, 12791-12811.
Reynolds, S., Mildren, S., Hillis, R., Meyer, J.J., Flottmann, T., 2005. Maximum horizontal stress orientations in the Cooper Basin, Australia: implications for plate-scale tectonics and local stress sources. Geophysis Journal International 150, 331-343.
Reynolds, S.D., Mildren, S.D., Hillis, R.R., Meyer, J.J., 2006. Constraining stress magnitudes using petroleum exploration data in Cooper-Eromanga basins, Australia. Tectonophysics 415, 123-140.
Short, K.C., Stauble, A.J., 1967. Outline of geology of Niger Delta. American Association of Petroleum Geologists Bulletin 51, 761-779.
Sibson, R.H., 1996. Structural permeability of fluid-driven fault-fracture meshes. Journal of Structural Geology 18, 1031-1042.
Stoneley, R., 1966. The Niger Delta region in the light of the history of continental drift Geology Magazine 103, 385-397.
Streit, J.E., Hillis, R.R., 2004. Estimating fault stability and sustainable fluid pressures for underground storage of CO_2 in porous rock. Energy 29, 1445-1456.
Tingay, M.R.P., 2011. Personal communication with Tingay, M. R. P. on the estimations of vertical stress and pore pressure, formerly of University of Adelaide, Australia, now at Chevron, Australia.
Tingay, M.R.P., Hillis, R.R., Morley, C.K., Swarbrick, R.E., Okpere, E.C., 2003. Variation in vertical stress in the Baram Basin, Brunei: tectonic and geomechanical implications. Marine and Petroleum Geology 20, 1201-1212.
Tingay, M.R.P., Hillis, R.R., Swarbrick, R.E., Morley, C.K., Damit, A.R., 2009. Origin of overpressure and pore-pressure prediction in the Baram province, Brunei. American Association of Petroleum Geologists Bulletin 93, 51-74.
Trudgill, B.D., Cartwright, J.A., 1994. Relay ramp forms and normal fault linkages - Canyonlands National Park, Utah Geological Society of America Bulletin 106, 1143-1157.
Tuttle, M.L., Charpentier, R.R., Brownfield, M.E., 1999. Preliminary report of the Niger Delta Petroleum System: Niger Delta Province, Nigeria, Cameroon, and Equatorial Guinea, Africa. 719201.
Waite, W.F., Santamarina, J.C., Cortes, D.D., Dugan, B., Espinoza, D.N., Germaine, J., Jang, J., Jung, J.W., Kneafsey, T.J., Shin, H., Soga, K., Winters, W.J., Yun, T., 2009. Physical properties of hydrate-bearing sediments. Reviews of Geophysics 47, RG4003.
Weber, K.J., 1987. Hydrocarbon distribution patterns in Nigerian growth fault structures controlled by structural style and stratigraphy. Journal of Petroleum Science and Engineering 1, 91-104.
Weber, K.J., 1971. Sedimentological aspects of oil field in the Niger Delta. Geologie en Mijnbouw 50, 559-576.
Weber, K.J., Daukoru, E.M., 1975. Petroleum geological aspects of the Niger Delta. Nigeria Journal of Mining and Geology 12, 9-22.
Webster, M., O'connor, S., Pindar, B., Swarbrick, R., 2011. Overpressures in the Taranaki Basin: Distribution, causes, and implications for exploration American Association of Petroleum Geologists Bulletin 95, 339-370.
Whiteman, A., 1982. Nigeria: Its Petroleum Geology, Resources and Potential. Graham and Trotman, London.
Yamashita, F., Fukuyama, E., Omura, K., 2004. Estimation of fault strength: Reconstruction of stress before the 1995 Kobe earthquake. Science 306, 261-263.
Ziegler, P.A., 1992. Plate tectonics, plate moving mechanisms and rifting, in Ziegler, P.A. (Ed.), Geodynamics of Rifting, 213 ed. Tectonophysics, pp. 203-225.
Zoback, M.D., 2010. Reservoir Geomechanics. Cambridge University Press, The Edinburgh Building, Cambridge, CB2 8RU, United Kingdom.
Zoback, M.D., Healy, J.H., 1984. Friction, faulting, and "in situ" stresses. Annales de Geophysique 2, 689-698.

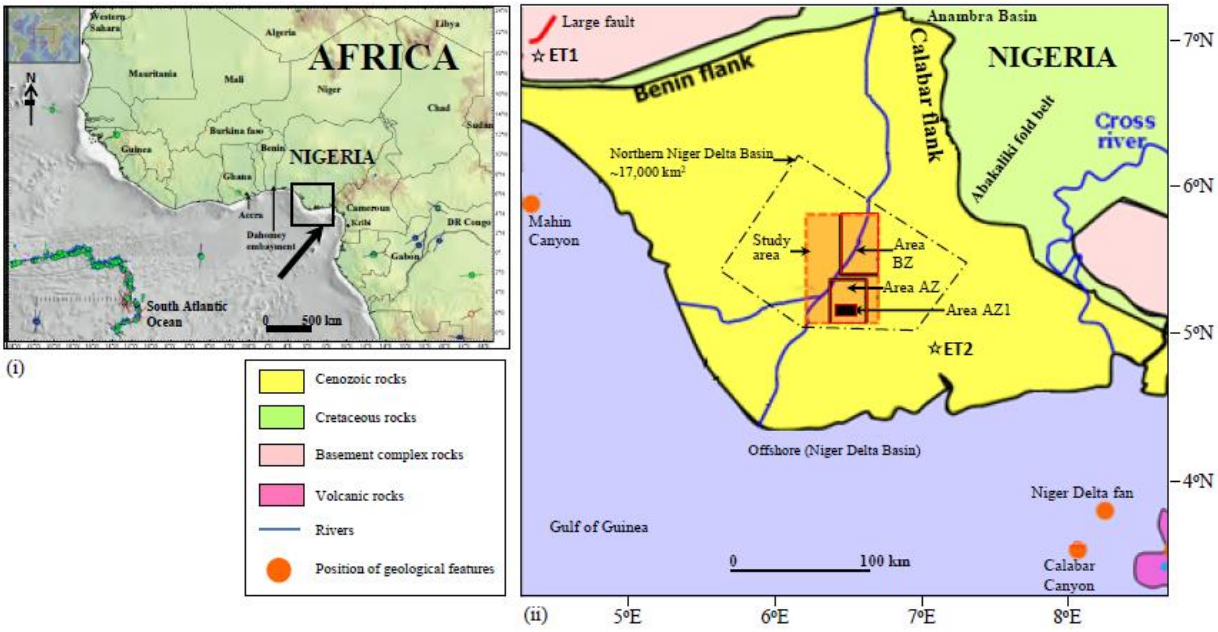

Figure 1. (i) The position of the Niger Delta Basin, Nigeria is shown in the box (in thick arrow). The stress directions (in green and blue lines) are from Heidbach et al. (2008). Topographic and bathymetric data in the background are taken from GeoMapApp (2014). (ii) The zoom in of the box shown in (i). The pentagon (black long dash dot line) approximates the area referred to as the NNDB. The position of the study area is verged in dash line. Other major sedimentary basins (Whiteman, 1982) are coloured light green and yellow on the map. Geological features in filled orange circles are from GeoMapApp (2014). The 5-Points stars (ET1 and ET2) represent approximate locations of the increased earth tremors referenced in the subsection 5.4. The legend for this map is shown on the bottom left.

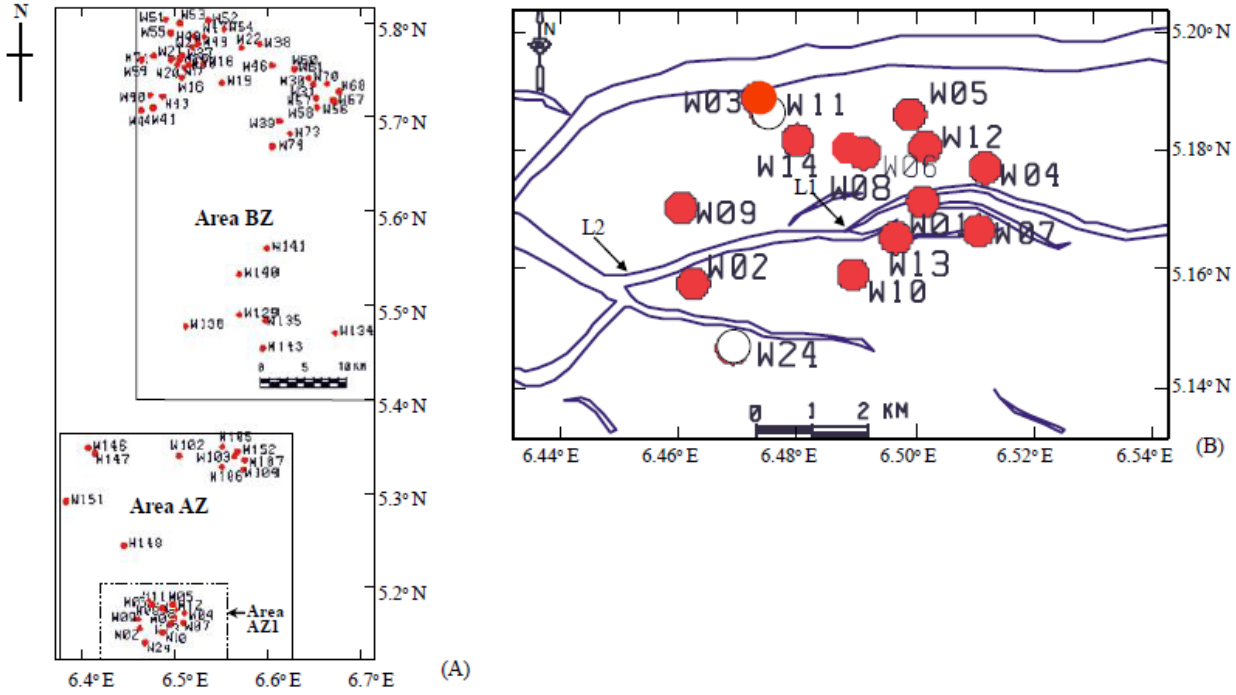

Figure 2. (A) displays the study area; Fig. 1(ii), and positions of 87 wells (in small filled red circles). (B) The zoom of the Area AZ1 shown in (A), which contains the 13 wells (in big filled red circles) studied in detail. The fault elements in the background are from Adewole and Healy (2013). Fault connections observed from 3D seismic data are: L1 = Soft link; L2 = Hard link.

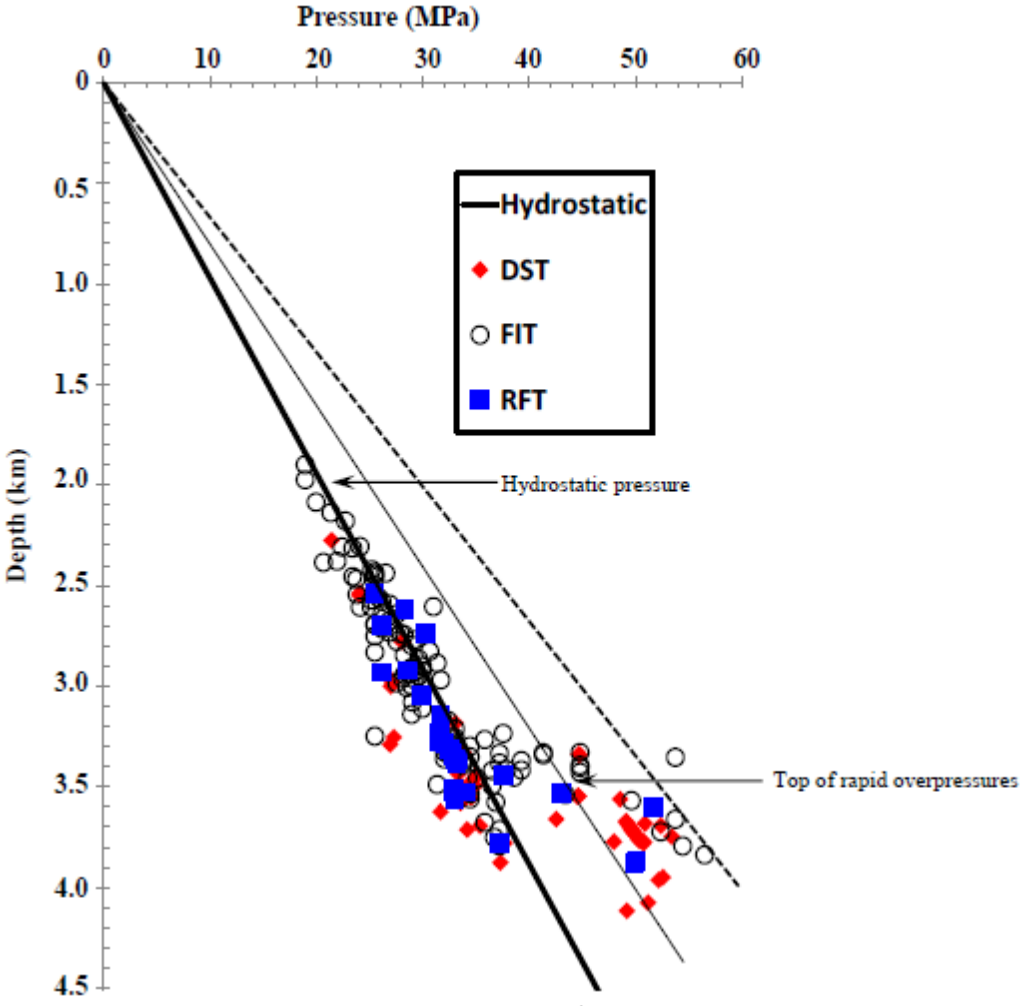

Figure 3. Pore pressure-depth profiles in the normal and overpressure wells in the NNDB from Adewole et al. (2016). The positions of these wells are presented in Figure 2. Pore pressure generally increases with depth, but becomes rapid at 3.5 km and increases exponentially at 4 km towards the fracture gradient. DST = Drilling Stem Test; FIT = Formation Integrity Test; RFT = Repeat Formation Test.

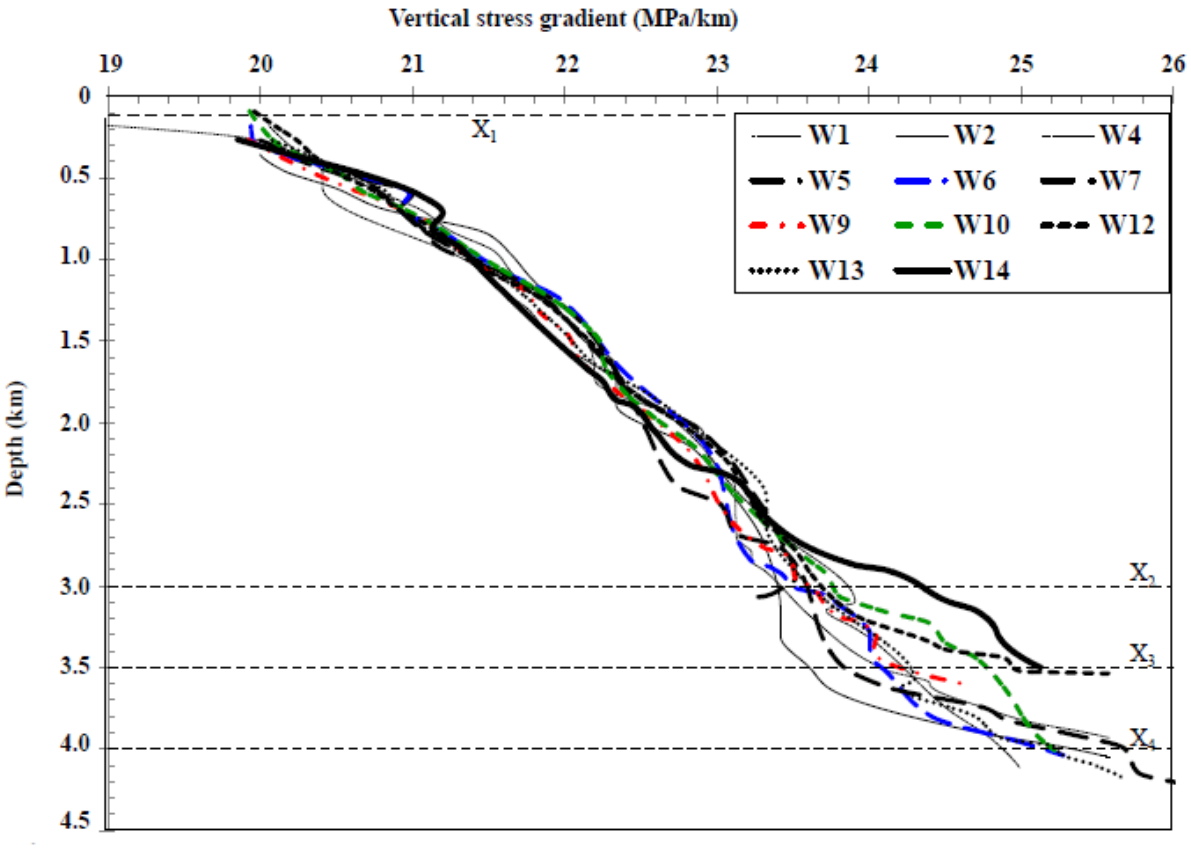

Figure 4. Examples of depth-vertical stress gradients crossplots for 11 wells shown in Figure 2(B). Vertical stress gradient increases with depth vertically, but varies horizontally across wells (easily seen from 3 km and above). The depth positions marked X_2, X_3, and X_4 are consistent with the tops of significant overpressure, rapid overpressure, and extreme overpressure respectively (Adewole et al., 2016).

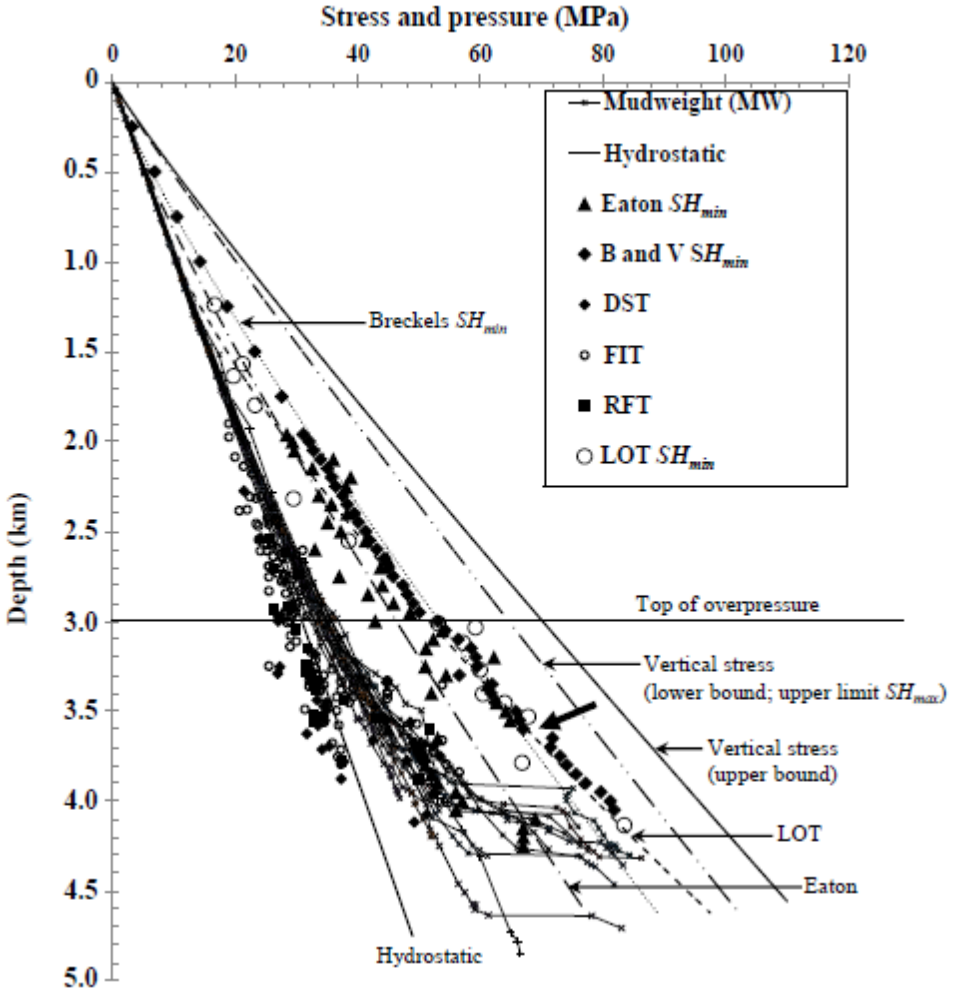

Figure 5. Pressure tests from wells (Figure 2) and the estimated full stress tensor as a function of depth in the NNDB (Adewole and Healy, 2013). The mud weight data have been used here as guides only for the pressure measurements. Note the tracking of the LOT line by the Breckels SH_{min} is indicative of the suitability of both methods in the basin. B and V = Breckels and Van Eekelen; DST = Drilling Stem Test; FIT = Formation Integrity Test; RFT = Repeat Formation Test; LOT = Leak-Off Test.

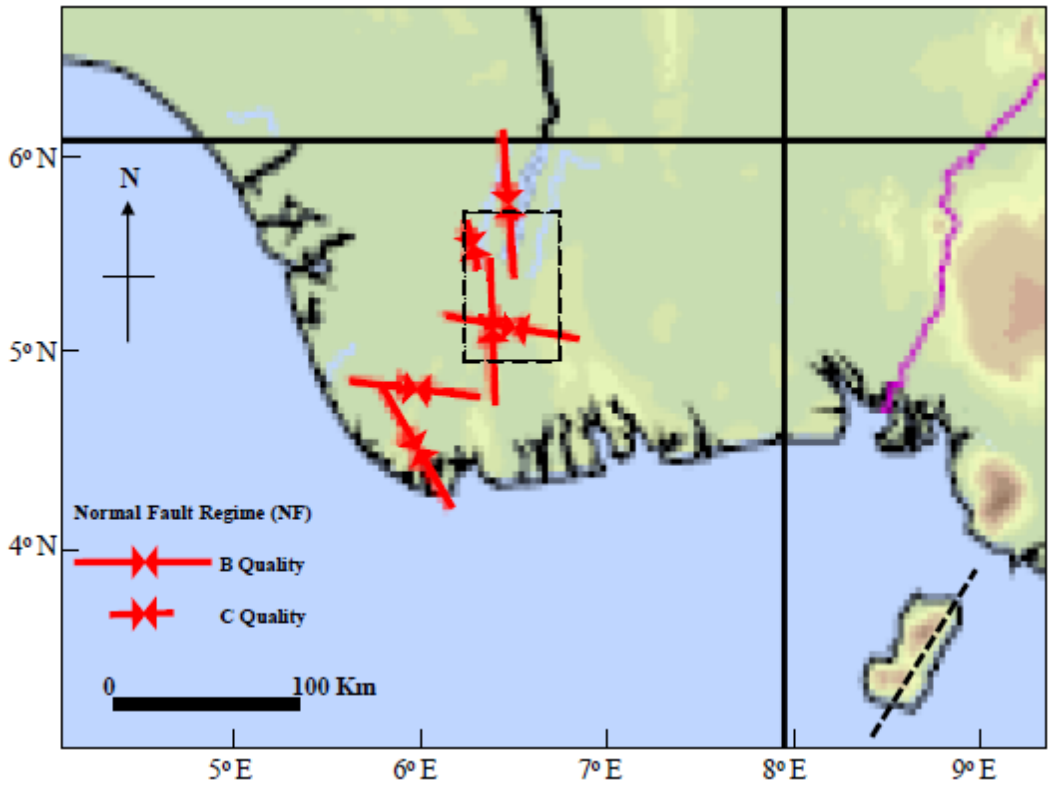

Figure 6. Results of the analyses of 39 borehole breakouts from 6 wells showing SH_{max} directions at the well locations in the Niger Delta Basin (Figures 1 and 2). Dark brown patches on the map are suggestive of high topographic measurements whereas, the light green and light yellow signify relatively lower measurements. The length of the stress direction arrows is a function of the quality of the dataset: (i) short arrow = lower quality (C); (ii) long arrow = higher quality (B).

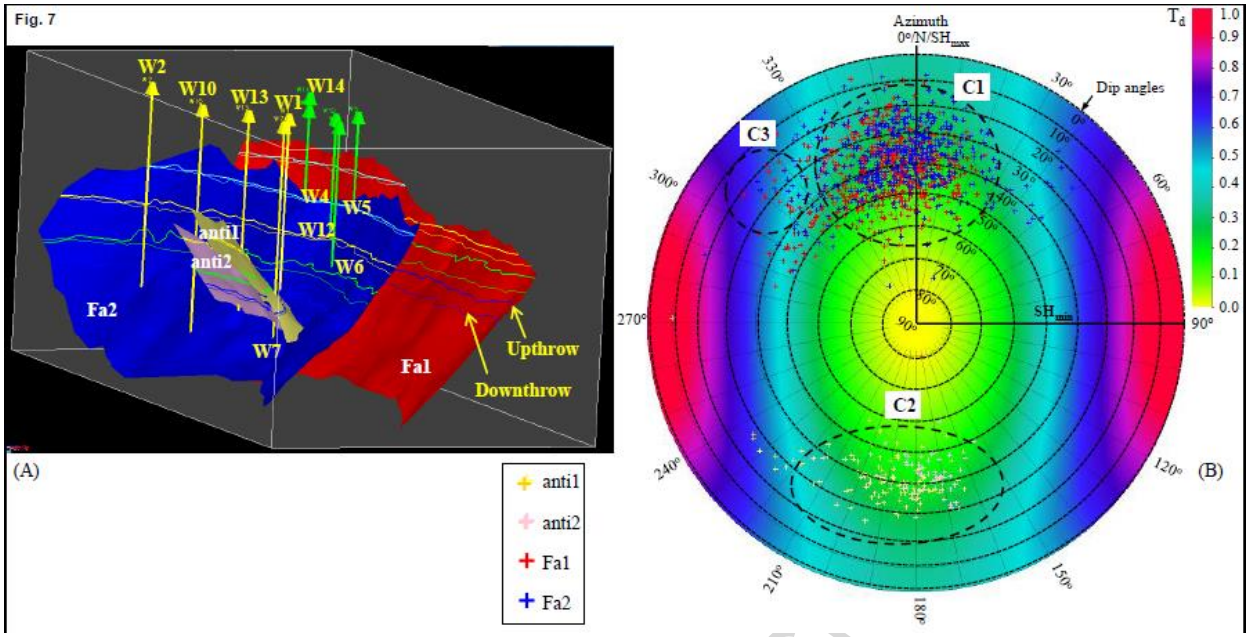

Figure 7. (A.) showing a 3D visualisation of the normal faulting surfaces (Fa1, Fa2, anti1, and anti2) interpreted from 3D seismic data; area AZ1, Figure 2. The legend of the fault segments symbolised in (B) is shown below (A). (B) demonstrating a stereonet with T_d data estimated from a normal faulting regime at 2 km, and 0° SH_{max} direction. Dip azimuth values (0° to 360°) are represented by long bars from the centre to the surface. The mean T_d value of the fault segments inside areas C1 and C2 is approximately ≤ 0.5, which is suggestive of a high structural stability in the SH_{max} direction given other favourable conditions (see Table 1 for the model parameters). Area C3 contrastingly meets the criteria for unstable faults; T_d values > 0.5. The range of the C3 on the stereonet is in the region of: azimuth = 300° - 322°; dip = 10° - 40°.

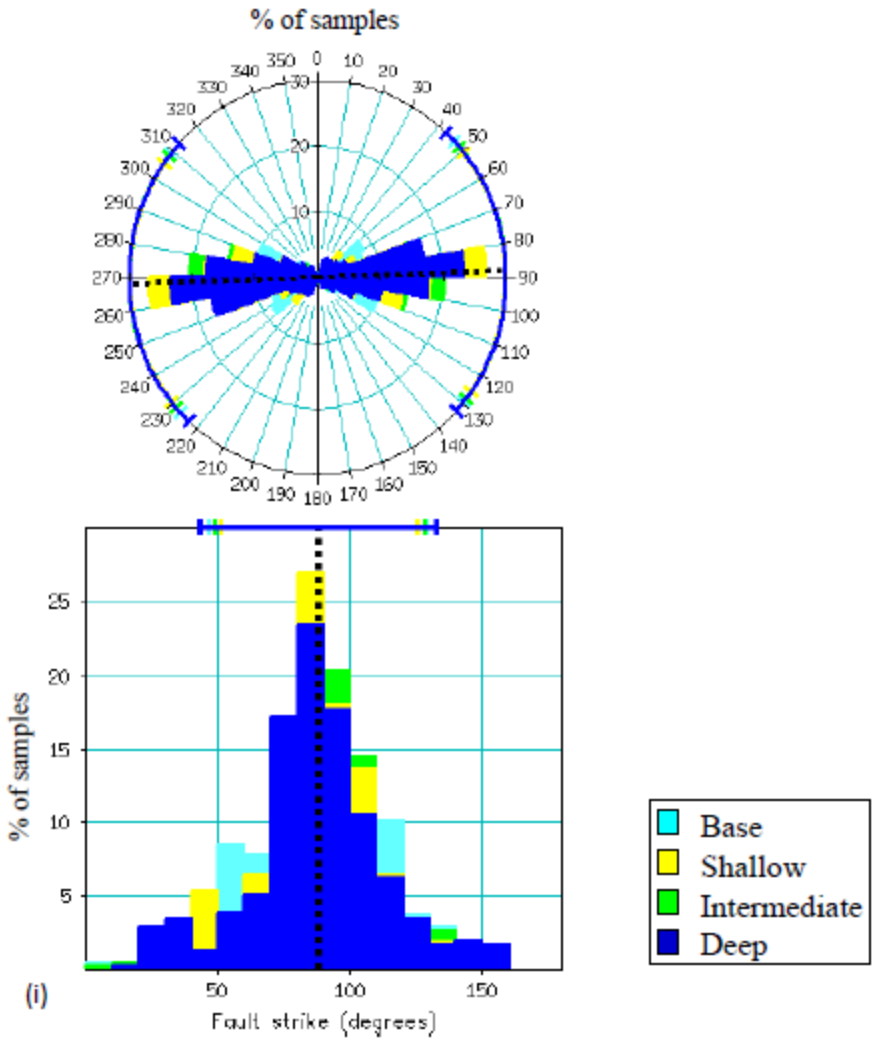

Figure 8. The depth of interpreted horizons from the 3D seismic data (area AZ1, Figure 2) increases from the base to the deep (Adewole and Healy, 2013). The legend of the horizons is on the right. Generally, the faults show a near horizontal uniform strike direction. By implication, a near vertical dip azimuth.

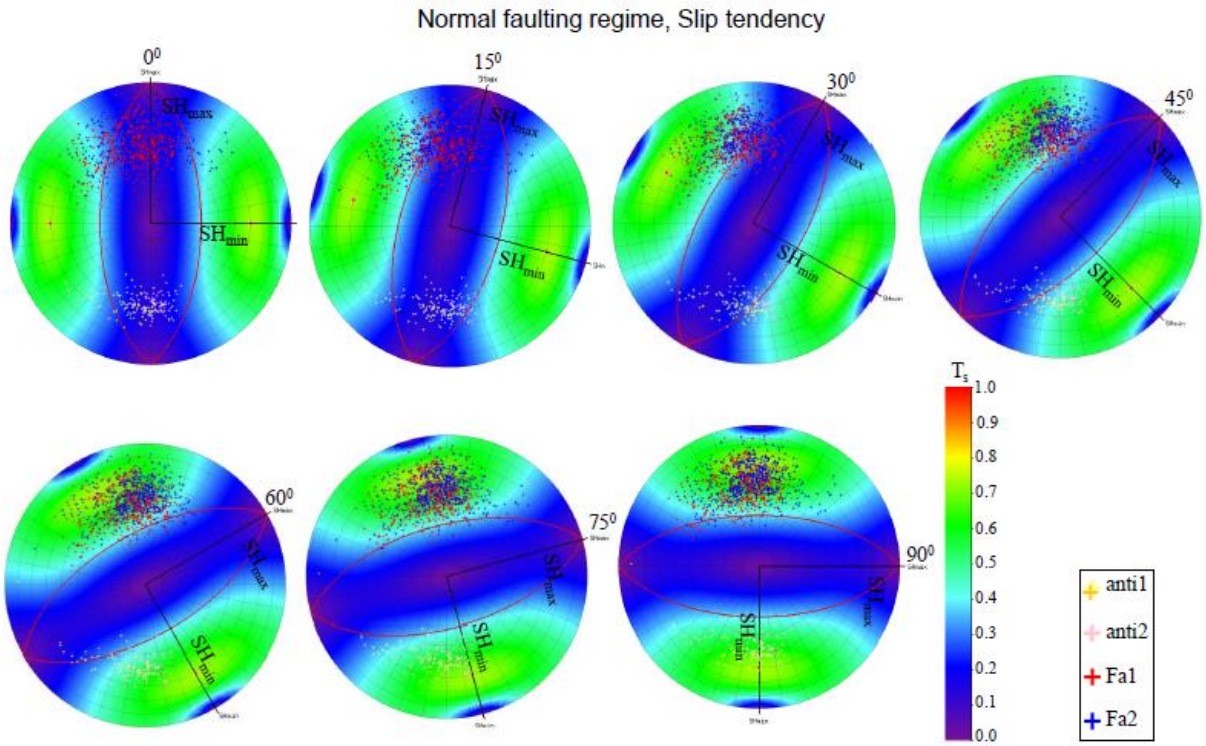

Figure 9. Stereonets demonstrating the estimated slip tendency attribute in a normal faulting regime at 2 km depth to show the relationship of changes in the SH_{max} direction to the stability of fault segments (the legend is shown in the extreme bottom right). T_s values greater than 0.6 on the stereonets signify a suitable condition for a slip to take place. Fault surfaces are more prone to a slip here from 30° SH_{max} orientation, but become serious at 60°, and approach a critical state of instability at 90° given other conditions (pressure and fault orientation). The model parameter for the scenario one presented here is shown in Table 1.

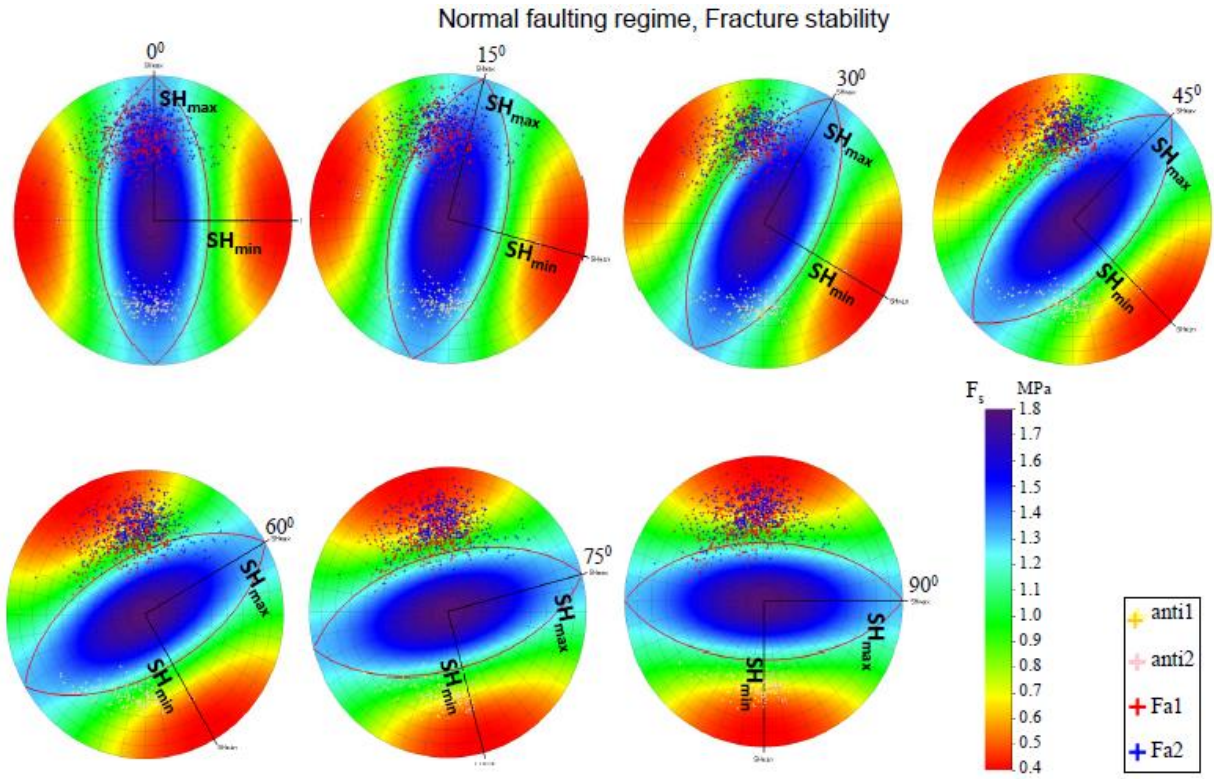

Figure 10. Stereonets showing results of evaluations of the fracture stability at 2 km depth in a normal faulting setting using scenario one parameters (Table 1). The legend for clustered fault segments on the surface of the stereonets are presented bottom right. The coloured F_s suggests increasing fault stability (F_s > 0.8 MPa) from 30° to 0° SH_{max} directions. However, a rapid decreasing F_s (< 0.8 MPa) is observed from 30° to 90°, signifying a potential lower structural strength.

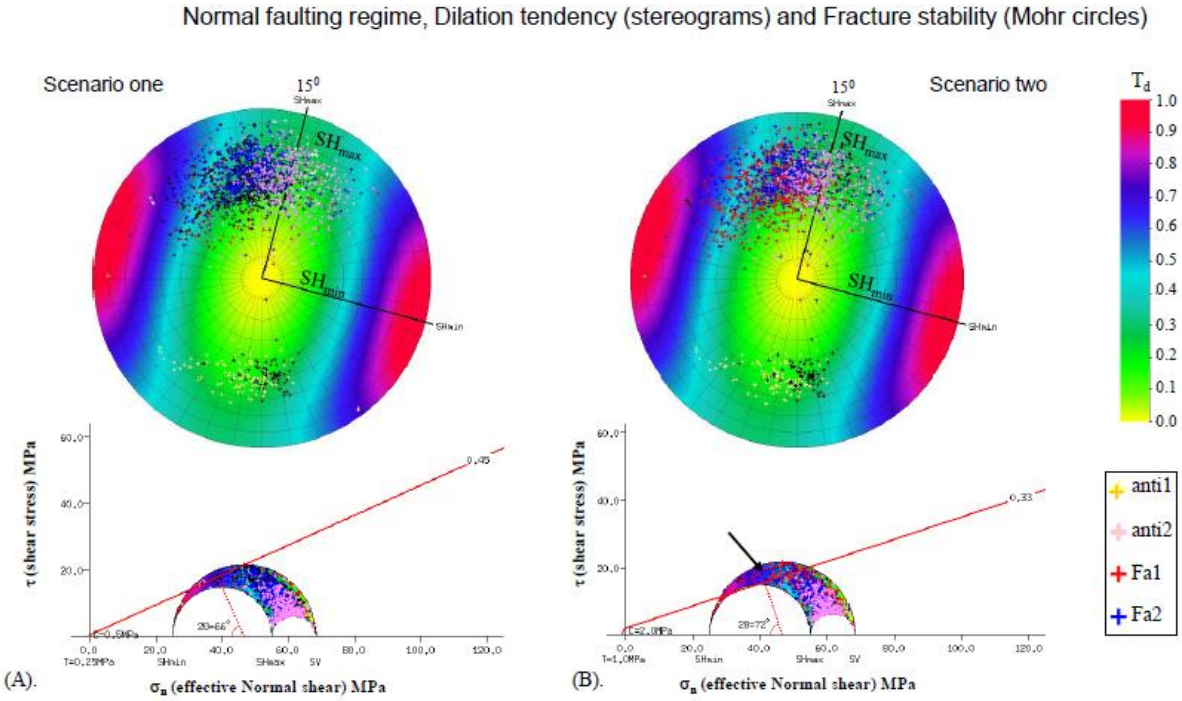

Figure 11. The stereograms (top) show the dilation tendency estimated at 3.5 km depth (normal faulting regime) in scenarios one (A) and two (B); Table 1. The fracture stability results are presented on the Mohr circles (bottom). Near similarities in the scatterings of the *Td* and *Fs* on the surfaces of the stereograms and Mohr circles respectively show true reflections of the same stress (dilation tendency) and pressure (fracture stability) data applied to the scenarios. However, apparent differences in the shear failure properties of the scenarios caused some of the fault segments to move from their presumed stable positions (below the Coulomb failure line; A) to the failure mode (above the Coulomb failure line; black arrow in B).

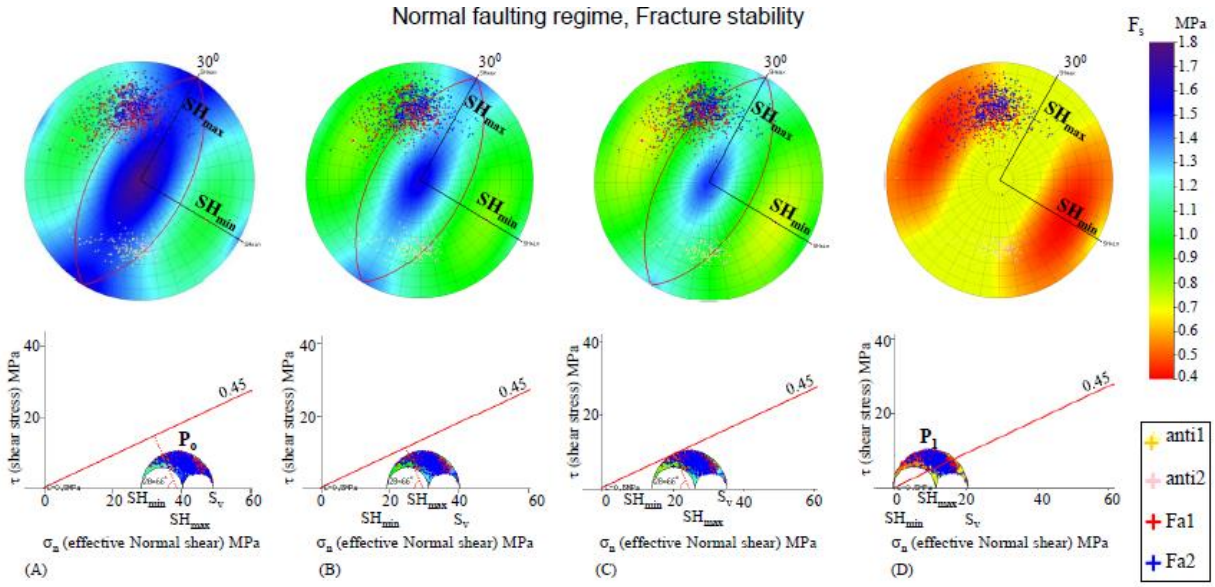

Figure 12. Stereograms and associated Mohr diagrams illustrating F_s models of the: (A) low pressure (36 MPa); (B) average pressure measurement from wells (45 MPa); (C) peak stable pressure (50 MPa); and (D) high pressure (65 MPa), demonstrating the effects of increasing pressures on the fracture stability in the normal faulting regime at 3.5 km depth. At elevated pore pressure equals or greater than 50 MPa, the stability of the faults are likely to be greatly compromised in the area. Model parameters for scenario one applied here are shown in Table 1. The legend of the fault segments is presented right of (D).

Fig. 13

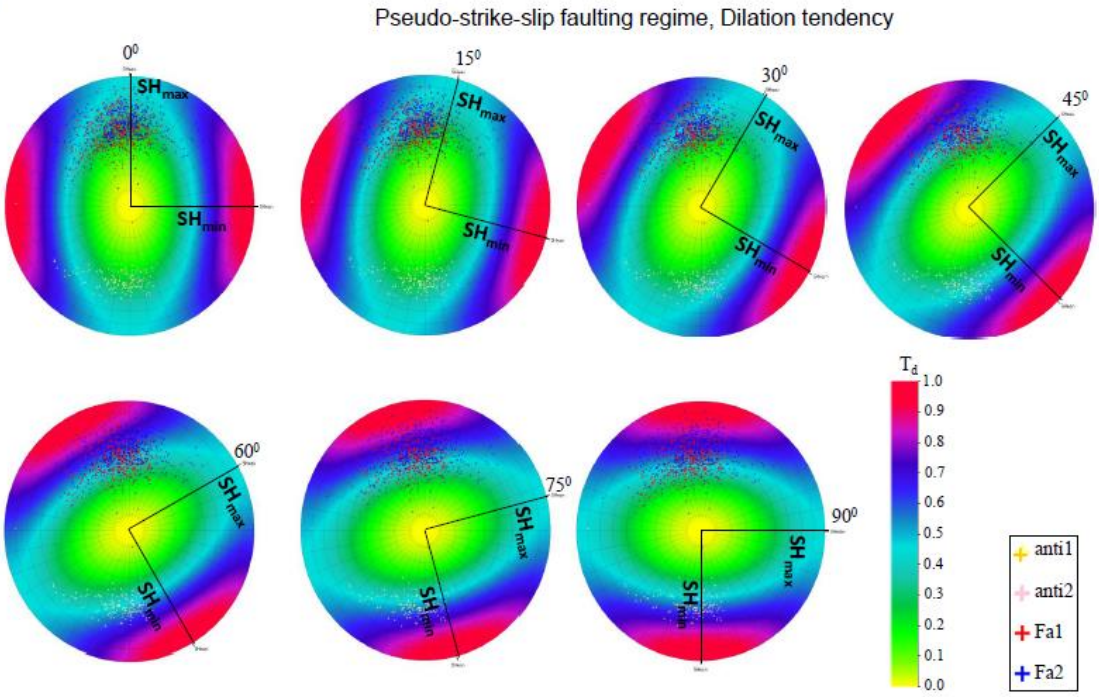

Figure 13. Examples of stability models in pseudo-strike-slip faulting regime. Dilation tendency data obtained at 4 km depth for different SH_{max} directions are presented on the stereonets. Increasing the SH_{max} direction also correspondingly decreasing the fault stability as observed in other faulting regimes in this study. Parameters for the scenario one models applied here are given in Table 1.

Fig. 14

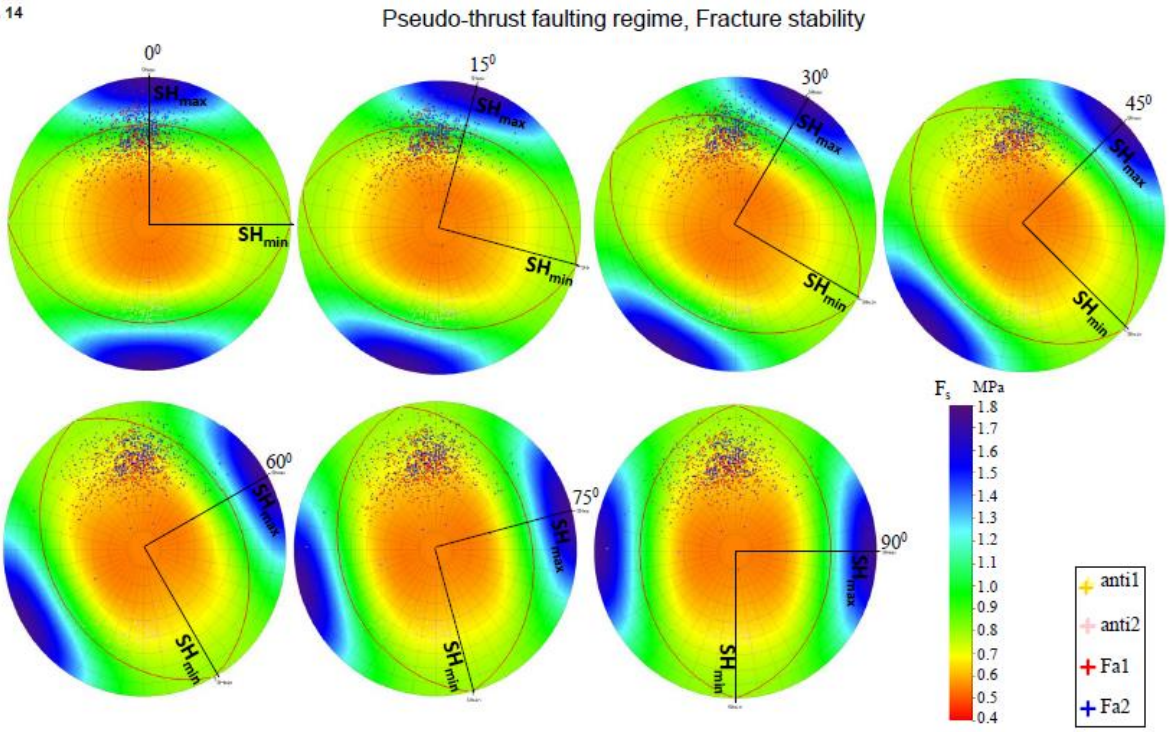

Figure 14. Pseudo-thrust faulting models generated at 4 km depth using the parameters in Table 1 (scenario one). F_s values deviating too much below 0.8 MPa have been assumed in all probability (favourable to other failure conditions such as orientation and stress magnitudes) to be potentially in failure modes.

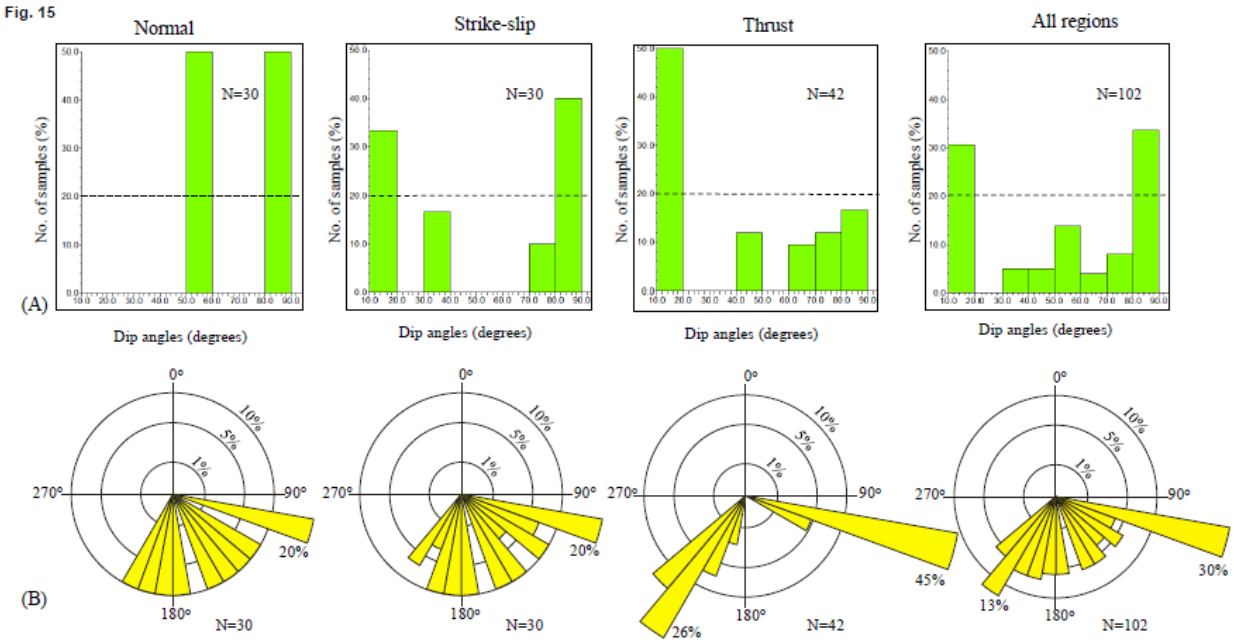

Figure 15. (A) Histograms of the fault dips and their corresponding (B) azimuths (rose plots) showing assessed instability directions in all the faulting regimes. (B) The length of the petals (shaded yellow) is indicative of the percentage of sampled data (in concentric circles). The dashed lines in (A) statistically represent 20% of sampled data. In general, the faults are in the highest risk directions for failure between 10^{o} - 20^{o} and 80^{o} - 90^{o} fault dips, and 100^{o} – 110^{o} azimuths in all the faulting regimes (≥ 20% total sampled data; 102). The azimuth values on the rose plots are in degrees. N=Number of sampled data.

Highlights

- We assessed fault stability in the dominant normal and two pseudos faulting regimes
- The use of Stability Indices for evaluations reveal potential failure directions
- Fault stability is compromised by high angles maximum horizontal stress directions
- High pore pressure, stress and right fault - stress direction reduce fault strength
- We proposed preoperational fault stability evaluations for hydrocarbon exploration